Received December 3, 2015, accepted December 25, 2015. Date of publication xxxx 00, 0000, date of current version xxxx 00, 0000.

Digital Object Identifier 10.1109/ACCESS.2015.2513010

INVITED PAPER

Video Streaming in the Multiuser Indoor Visible Light Downlink

JUNYI JIANG, YONGKAI HUO, FAN JIN, PEICHANG ZHANG, ZHAOCHENG WANG, (Senior Member, IEEE), ZHENGYUAN XU, HARALD HAAS, AND LAJOS HANZO, (Fellow, IEEE)

Electronics and Computer Science, University of Southampton, Southampton SO17 1BJ, U.K.

Corresponding author: L. Hanzo (lh@ecs.soton.ac.uk)

AQ:1 This work was supported in part by the U.K. Engineering and Physical Sciences Research Council within the India-U.K. Advanced Technology Centre through the European Concerto Project under Grant EP/Noo4558/1 and in part by the European Research Council Advanced Fellow Grant through the Beam-Me-Up Project.

ABSTRACT Indoor visible light communication (VLC) using a light emitting diode (LED) transmitter provides a high-signal-to-noise (SNR) link, which is ideal for video transmission. The LED lights illuminate their own attocells and convey video streams in the downlink to multiple mobile terminals (MTs). Three different transmission schemes are considered, namely: the unity frequency reuse, the higher frequency reuse factor-based transmission, and the novel vectored transmission. We then formulate the optimization problems aiming at minimizing the video distortion. This paper commences by evaluating the performance of the MT at specific positions and continues by characterizing the peak SNR (PSNR) degradation across the room. Finally, we quantify the average performance of multiple MTs randomly walking in the room. By investigating the PSNR degradation, the video rate achieved, the energy consumed, and the effects of buffering delay on the video distortion, we demonstrate that the proposed VLC system is capable of supporting high-quality multimedia transmissions.

INDEX TERMS Video frames, PSNR degradation, achieved video rate, VLC, VT-2.

NOMENCLATURE

2D	2-Dimensional
5G	Fifth Generation
ACO-OFDM	Asymmetrically Clipped Optical OFDM
ADO-OFDM	Asymmetrically Clipped DC-bias Optical OFDM
CIR	Channel Impulse Response
COWA	Centre on Optical Wireless Applications
CSK	Colour Shift Keying
DCO-OFDM	DC-biased Optical OFDM
DL	Downlink
FFR	Fractional Frequency Reuse
FOV	Field-of-View
FPS	Frame per Second
GOP	Group-of-Picture
GSSK	Generalised Space Shift Keying
HetNet	Heterogeneous Networks
HFRFT	Higher Frequency Reuse Factor based Transmission
ISI	Inter-Symbol Interference
ITU	The International Telecommunication Union
LED	Light Emitting Diode
LOS	Line-of-Sight
LTE	Long Term Evolution
MC-LED	Multi-Chip LED
MMW	Millimeter-Wave
MSE	Mean Square Error
MMSE-DFE	Minimum MSE - Decision Feedback
MT	Mobile Terminal
NOMAD	Nolinear Optimisation by Mesh Adaptive Direct Search
OOK	On-Off Keying
OLED	Organic LED
OMEGA	hOme Gigabit Access

OW	Optical Wireless
PAM-DMT	Pulse Amplitude Modulation based Discrete Multitone
PC-LED	Phosphor Converted LED
PD	Photodetector
PPM	Pulse Position Modulation
PSNR	Peak Signal-to-Noise Ratio
RF	Radio Frequency
SINR	Signal-to-Interference-plus-Noise Ratio
SLERC	Smart Lighting Engineering Research Center
SNR	Signal-to-Noise Ratio
TPC	Transmission Precoding
UC-Light	Ubiquitous Communication by Light
UFR	Unity Frequency Reuse
VLC	Visible Light Communication
VLCC	VLC Consortium
VT	Vectored Transmission
WCDMA	Wideband Code Division Multiple Access
WPAN	Wireless Personal Area Network
ZF	Zero-Forcing
μ-LED	Micro-LED

I. INTRODUCTION

Represents the next phase of mobile communication, which is the subject of intensive research around the world. Whilst the Long Term Evolution (LTE) system has been rolled out in the large parts of the globe, the 5G system is expected to provide ubiquitous access to information anywhere and anytime for anyone and anything [1]–[3]. The recent concept of Heterogeneous Networks (HetNet) constitutes a beneficial structural evolution towards the 5G system concept, while the exploration of both Millimeter-Wave (MMW) and Optical Wireless (OW) networks [4], [5] opens up further emerging venues. In the OW regime, apart from the already well-documented Infrared region of the optical spectrum [6], high data rate Visible Light Communication (VLC) exemplified in the stylized illustration of Fig. 1 [11] has become a reality in indoor environments [7].

Naturally, the VLC atto-cells have their specific propagation characteristics, which are often modelled by a simple line-of-sight (LOS) Gaussian channel within the reveiver's specific Field-of-View (FOV). They also tend to have a limited propagation distance, as exemplified in the scenario of Fig. 1, where the Light-Emitting Diodes (LED) act as transmitters. The simplest solution is to flicker the LEDs according to the binary zeros and ones to be transmitted, where the received impulses can be detected by a photo-diode. These LED transmitters might be linked up for example by the power-line network constituted by the mains cables, which constitute by no means a perfect communications network, since they have not been designed for telecommunications. Hence they have a limited bandwidth, therefor imposing both dispersion as well as impulsive noise. Nonetheless, in this treatise we will stipulate the idealized simplifying assumption that the LEDs are linked up by a perfect backbone network. The impairments of this power-line network and a range of countermeasures were detailed

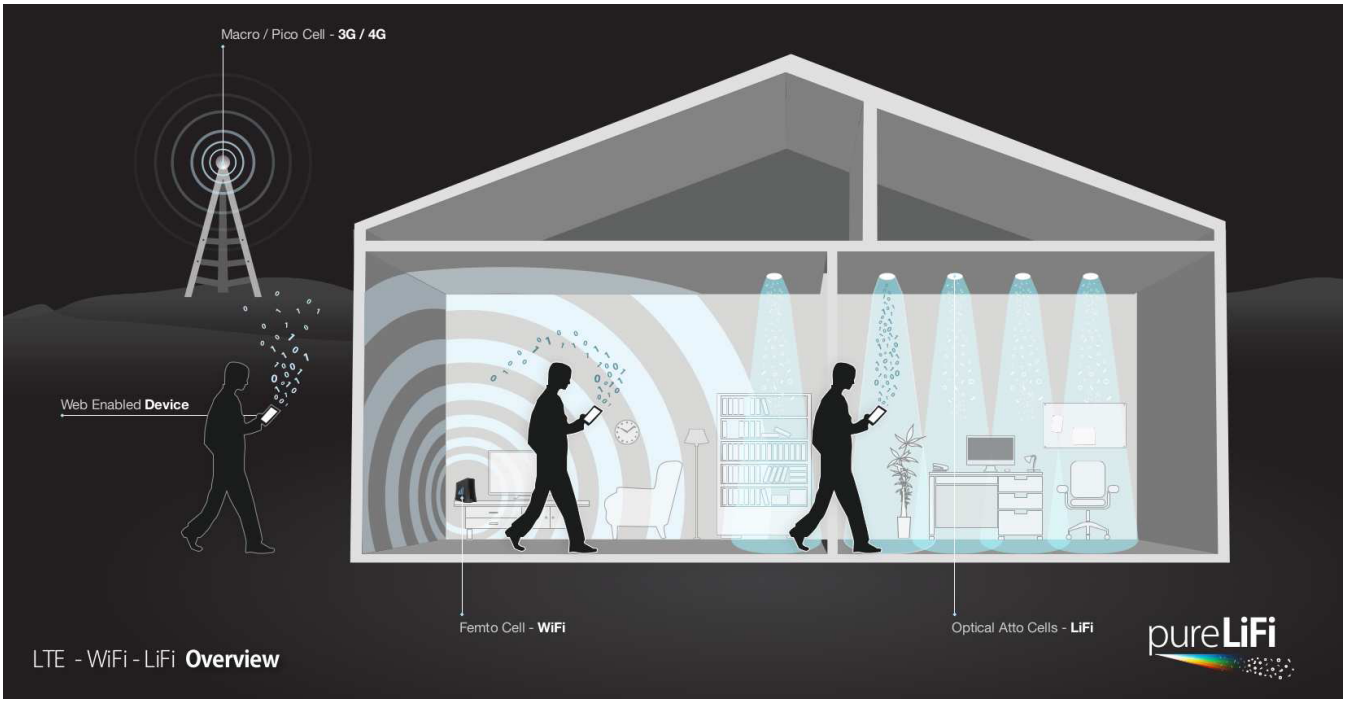

FIGURE 1. A stylized indoor VLC system [11].

for example in [8]. However, this VLC transmission regime is less suitable for the uplink, which is fortunately amenable to classic radio-frequency (RF) transmission, as discussed for example in [9].

The family of VLC systems exhibits several beneficial characteristics, such as inherent information security, a vast bandwidth in the unlicensed spectrum band, low-cost Light Emit Diode (LED) based transmitters and Photodetectors (PDs)), etc. On the other hand, as seen in Fig. 2, the investigations of Cisco concerning the global mobile data traffic forecast for 2014 to 2019 [10] have shown that video transmission is and will continue be the most dominant tele-traffic type [10]. Hence, VLC is especially suitable for high-quality multimedia video transmission, as one of its 'killer' applications.

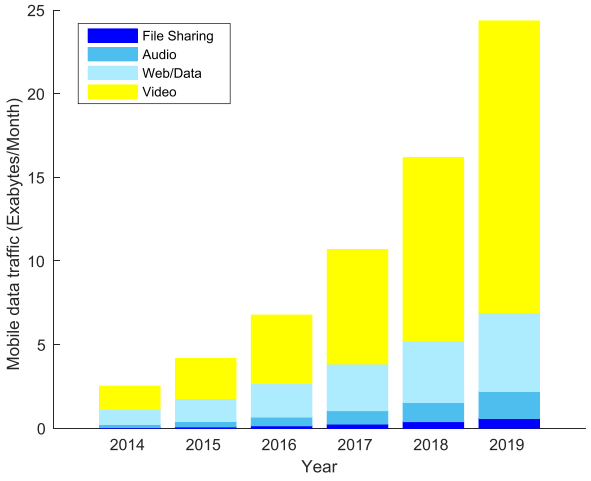

FIGURE 2. **The global mobile data traffic forecast for 2014 to 2019 [10].**

More specifically, video streaming has become a popular wireless service and hence it has been widely studied in conventional RF systems from various perspectives [12]–[18], [21]. In [12], the problem of choosing the best streaming policy under both bandwidth and playback delay constraints is addressed, whilst resource allocation and packet scheduling is studied in [13]. In [14], the rate based fairness of video flows is studied, while the problem of scheduling delay-sensitive media-sources, such as lip-synchronised video is considered in [15]. The content-aware optimisation of a Wideband Code Division Multiple Access (WCDMA) system in proposed in [16], where the authors use the Peak Signal-to-Noise Ratio (PSNR) for characterising the video distortion. Furthermore, a novel distortion estimation parameter referred to as the 'distortion impact' was proposed in [17]. Finally, the subject of content-aware video transmission is investigated in the context of HetNets in [18].

Designing content-aware video streaming in VLC systems is non-trivial, since the VLC system transmission are highly directional. This results into confined coverage of VLC cells, which are also referred to as ''attocells''. In this context, the initial study of [4] analysed the fundamental factors affecting the performance of the VLC system, assuming that all the LEDs in the system illuminate a single attocell. This appealing simple philosophy provides a reliable coverage without imposing interference, but the price to pay is that, the system is only capable of serving a single Mobile Terminal (MT) in a transmission slot. A simple and straightforward way of circumventing this disadvantage is to arrange for every single LED light to create and illuminate its own attocell and to simultaneously serve a multiplicity different MTs requesting different traffic. However, the ubiquitous inter-cell interference between the neighbouring attocells formulated by the neighbouring LED lights imposes detrimental effects on the MTs at the attocell edge. In order to solve this problem, more sophisticated transmission regimes have to be conceived. At the time of writing, there is paucity of studies on the transmission schemes conceived for VLC cells. The authors of [19] discussed the so-called Fractional Frequency Reuse (FFR) scheme, which strikes a compromise between the cell-edge MT performance and the system throughput, whilst maintaining a low system complexity. Subsequently, a joint multi-user transmission regime was discussed in [9] and [20], which relies on concurrent data transmission from multiple cooperated LED points to a MT in the Down Link (DL). Whilst the design of the VLC transceivers has recently received substantial research attention, apart from [40]–[43] there is a paucity of literature related to the holistic design audio and video streaming VLC systems.

Against this background, we commence by briefly reviewing the advances both in VLC and in video compression, followed by the holistic design of a VLC-based video streaming system. More explicitly, given the paucity of literature on the design and performance characterization of VLC-aided video systems, our contribution is that we conceive and optimise an indoor VLC system for video streaming relying on both classic Unity Frequency Reuse (UFR) as well as on Higher Frequency Reuse Factor based Transmission (HFRFT) and on Vectored Transmission (VT). Explicitly, we minimise the total video streaming distortion, whilst satisfying both the minimum rate constraints as well as the optical constraints. Finally, the video distortion, the video rate achieved and the energy consumed are quantified in the context of our optimisation problem.

The structure of this paper is shown in Fig. 3. In Section II, we briefly review the background of VLC systems, while in Section III we describe our channel model and a set of three transmission schemes, namely the above-mentioned UFR, HFRFT and VT regimes. The traffic model of video streaming and the formulation of our optimisation problem for multi-MT is detailed in Section IV. In Section V, our numerical results are discussed and our conclusions are provided in Section VI. Furthermore, the list of symbol is provided in the Appendix.

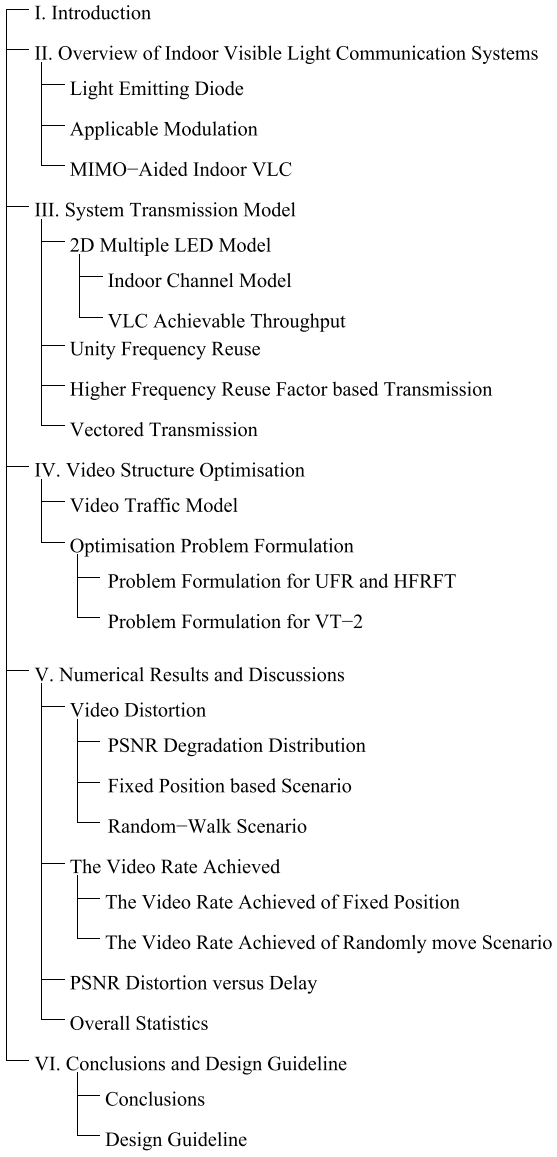

FIGURE 3. The structure of the paper.

II. OVERVIEW OF INDOOR VISIBLE LIGHT COMMUNICATION SYSTEMS

Let us start our review from the VLC systems relying on cutting-edge LED devices for transmitting data in the downlink as a potential solution to circumvent the spectrum shortage of RF communication systems. By combining the illumination and communication functions, VLC offers ubiquitous communication in indoor environments. VLC systems operates in the 4×10^{14} to 7.9×10^{14} [Hz] frequency bands, as shwon in Fig. 4. As in most OW communication systems, the information is transmitted by modulating the intensity of the signal at a rate substantially faster than the human eye's fusion frequency. Typically, photo-diode transmitters and DD receivers are employed. As a predominant optical source, the LED lights are exploited due to their unique advantages of high switching rate, energy efficiency and long-life characteristics. LEDs were developed in 1998 for transmitting

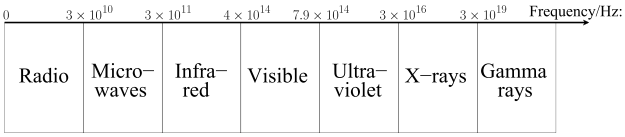

FIGURE 4. Stylised partitioning of the electromagnetic spectrum.

modulated optical signals [44]. In the early 2000s, the indoor VLC pioneers of Japan started to utilise white LEDs for both illumination and communication functions [4], [45]. The rapid development of VLC was supported by the VLC Consortium (VLCC) and it was also standardised [46]. In Europe, the hOME Gigabit Access (OMEGA) project was founded by a number of industrial partners aiming for transmitting at Gigabit data rates for domestic users [47], [48]. Additionally, a number of other research groups, including the Centre for Ubiquitous Communication by Light (UC-Light) [49], Centre on Optical Wireless Applications (COWA) [50], the Smart Lighting Engineering Research Center (SLERC) [51] have also contributed substantially. The first IEEE 802.15.7 VLC standard was published in 2011 for Wireless Personal Area Networks (WPANs) [52]. Hence in this section, we briefly review the indoor VLC concept.

A. LIGHT EMITTING DIODES

In indoor VLC links, due to their short distance, the Signal-to-Noise Ratio (SNR) of the system is typically high. The electromagnetic spectrum available in each room may be readily reused, thanks to the low penetration of external visible light. Given the wide availability of white LEDs [53]–[55], the indoor environments such as homes and offices constitute ideal schemes for combining indoor illumination with VLC.

Naturally, illumination remains the prime function of LEDs, which have the following advantages over traditional lighting:

- *Energy Efficient*: Compared to the obsolete incandescent bulbs, LEDs save up to 80% of energy, since they generate less heat [56].
- *Long Lifetime*: Compared to the 6,000 to 15,000 hours lifetime of conventional incandescent bulbs, LEDs ensure a longer service time of 25,000 to 50,000 hours [57].
- *High Luminous Efficacy*: Compared to the average luminous efficacy level of incandescent light bulbs (14 [lm/W]) and fluorescent lamps (75 [lm/W]), the novel InGaN based LEDs achieved a luminous efficacy of up to 254 [lm/W] in 2012 [58].
- *Moderately High Bandwidth*: LEDs have been developed to have up to 100 [MHz] bandwidth that could be invoked to support communication [47].
- *Multi-Functional Operation*: LEDs have the versatility to control the radiated spectrum, hence they are capable of producing high-intensity multi-coloured light [59].

Given the above impressive characteristics of LED lighting, it has drawn considerable attention in both the academic and

TABLE 1. A brief summary of major contributions on LED techniques.

Year	Authors	Contributions
2009	M. H. Crawford [53]	Described the advances in LED materials and novel devices
2009	H. Elgala *et al.* [54]	Proposed a novel VLC hardware prototype
2012	R. Mesleh *et al.* [55]	Proposed techniques of eliminating the non-linear distortion in a coded soft detection aided VLC system
2014	R. Zhang *et al.* [64]	Presented a wide range TRIAC-dimmable LED drivers
2014	I. Akasaki *et al.* [65]	Invent an efficient blue LED which enables bright and energy-saving white light source.
2015	T.-J. Liang *et al.* [66]	Proposed a novel LED driver having a current-limiting mechanism

industrial research communities in terms of indoor illumination, traffic lights and other light-related infrastructures.

In the current commercial market, there are diverse types of LEDs, such as the Phosphor Converted LEDs (PC-LEDs) [60], Multi-Chip LEDs (MC-LEDs) [61], Organic LEDs (OLEDs) [62] and Micro-LEDs (μ-LEDs) [63].

1) PC-LEDs

A white LED primarily using a single blue InGaN LED chip, where a layer of phosphor transforms blue light into green, yellow and red, which jointly produce white light [60]. To elaborate, the white light produced by the PC-LED can be classified into warm-white, neutral-white and cool-white, as determined by the thickness of phosphor. The bandwidth of PC-LEDs is relatively low.

2) MC-LEDs

They are constituted by three or more LEDs, individually emitting differently coloured light, usually red, green and blue to produce white light [61]. Colour control is achieved by adjusting the different intensities of the different colours. Compared to PC-LEDs, their complexity and cost is lower. Despite this, the MC-LED does not have a higher bandwidth than the PC-LED.

3) OLEDs

They are based on an organic layer sandwiched between positive and negative carriers in order to stimulate light emission. This LED is commonly used for panel displays. The limited frequency response of OLEDs makes them unsuitable for high-speed applications [62].

4) μ-LEDs

An AlGaN based LED array is typically used in VLC and optical fibre applications, which has great potential to be used for panel displays for the sake of supporting high-speed parallel communication. Additionally, they are capable of handling high light output densities, as a benefit of their substantial heat-sinking ability [63].

There are numerous contributions on LEDs [53]–[55], [64], [66]. In [53], the advances in LED materials and devices are detailed, while a white LED-based hardware prototype was designed for short range broadcasting in [54], where the authors focus their attention on the physical layer. In [55], various techniques compensating for the non-linear distortions are analysed and compared in a channel-coded soft detection aided VLC system. A novel clipping distortion reduction method was also proposed. The TRIAC-dimmable LED driver of [64] supports a wide dimming range. A range of dimming-control issues were investigated in [71] and [72]. The LED development-related studies have been summarised in a nutshell in Table 1.

B. APPLICABLE MODULATION SCHEMES

In VLC, the modulated signals can be used to switch the LEDs at a given frequency, which conveys the on-off pattern-based binary information to the receiver. The amplitude modulation schemes such as On-OFF Keying (OOK) and Pulse Position Modulation (PPM) are directly invoked in indoor VLC systems. Furthermore, by exploiting the more benign channel conditions of indoor VLC systems, some unique modulation schemes such as Generalised Space Shift Keying (GSSK) [67], Colour-Shift Keying (CSK) [5], [68] and Optical-OFDM, representing both DC-biased Optical OFDM (DCO-OFDM) [69] and Asymmetrically Clipped Optical OFDM (ACO-OFDM) [105] may be also used. In this subsection we will brief summarise the contributions that developed these three modulation schemes.

OFDM relies on multiple orthogonal subcarriers for the transmission of numerous low-rate parallel data stream. Explicitly, since the signalling symbol duration of each subcarrier is expanded according to the number of subcarriers, the duration of each of these subcarrier symbols is designed to become substantially longer than the typical channel impulse response. This is particularly true in the indoor VLC scenario considered, where typically only very mild dispersions prevail. Again, in VLC systems, the transmitted signals must be real and positive. To appropriately modify the OFDM scheme for employment in VLC systems, the concept of DCO-OFDM inspired by [73] may be employed, where a DC-bias is used for shifting the Optical OFDM modulated signal above zero. However, the disadvantages of DCO-OFDM, such as its undesired negative peak-clipping and its DC-related energy inefficiency motivated the design of ACO-OFDM, which does not suffer from the above-mentioned clipping problem [106]. The ACO-OFDM concept was proposed in [105], while its BER performance

TABLE 2. A brief summary of contributions on optical OFDM techniques.

Year	Authors	Contributions
2006	J. Armstrong *et al.* [74], [105]	Proposed ACO-OFDM and analysed its performance
2007	X. Li *et al.* [75]	Investigated the channel capacity of ACO-OFDM
2008	J. Armstrong *et al.* [69]	Characterised the analytical and simulation-based performance of both ACO-OFDM and DCO-OFDM
2008	S. Tian *et al.* [76]	Proposed a synchronisation method for ACO-OFDM
2009	J. Armstrong [77]	Presented a survey of Optical OFDM
2009	S. K. Wilson *et al.* [78]	Proposed a new constellation design for ACO-OFDM
2011	D. J. F. Barros *et al.* [79]	Compared the performance of various modulation schemes including ACO-OFDM and DCO-OFDM
2012	X. Li *et al.* [81]	Analysed ACO-OFDM from information theoretical perspective subject to various constraints
2012	R. Zhang *et al.* [83]	Multiple superimposed and spread layers of information were mapped to the subcarriers of ACO-OFDM and DCO-OFDM
2015	J. Jiang *et al.* [86]	Proposed an aperture selection aided ACO-OFDM based MIMO system

and capacity for transmission over AWGN channels were evaluated in [74] and [75] respectively. In [69], DCO-OFDM and ACO-OFDM were compared both in terms of their BER performance and bandwidth efficiency, whilst in [70] direct-detection assisted ACO-OFDM was investigated. As a further development, a synchronisation method was proposed for ACO-OFDM in [76]. A brief survey of Optical OFDM was provided in [77]. In [78], a novel sub-carrier-loading based constellation design was proposed for ACO-OFDM. In [79], various modulation schemes suitable for IM/DD were compared, including the OOK, DCO-OFDM, ACO-OFDM and PAM based Discrete Multitone (PAM-DMT) techniques. Diversity-combing assisted ACO-OFDM was advocated in [80]. The information theoretic characteristics of ACO-OFDM subject to a range of different constraints were analysed in [81]. In [82], ACO-OFDM and PAM relying on a Minimum Mean Square Error (MMSE) - Decision Feedback (DFE) equaliser for eliminating the dispersion were compared. Multiple superimposed and spread layers of information were mapped to the subcarriers of both ACO-OFDM and DCO-OFDM in [83], which were detected with the aid of a sophisticated turbo receiver. The system was capable of striking a flexible throughput versus robustness trade-off as a function of the number of superimposed layers. A hybrid Optical OFDM system combining some elements of both DC-biased and asymmetrically clipped techniques was conceived, which was hence referred to as Asymmetrically Clipped DC-bias Optical OFDM (ADO-OFDM) [84]. Another hybrid combination of ACO-OFDM and of PAM-DMT was proposed in [85], which struck a compromise. The Optical OFDM-related studies have been summarised in Table 2.

GSSK is a unique subset of the Spatial Modulation family [67], where $\log_2 M_{\text{sym}}$ bits may be conveyed by activating one out of M_{sym} signalling elements, as exemplified by an LED [87]. Compared to the conventional OOK and PPM modulation schemes, the GSSK technique exhibits a higher spectral efficiency [88]. Viewing them from a different perspectives, given the same spectral efficiency, the complexity of GSSK may be deemed to be lower than that of PAM. However, a specific impediment of GSSK is that its BER performance is highly channel-dependent, as demonstrated in [88].

C. MIMO-AIDED INDOOR VLC

Based on the maturing VLC studies [4], [89], [90] and on indoor channel modelling [45], [91], [92], the MIMO concept was introduced also into the family of VLC system [93], [94], where multiple transmitters and receivers supported a parallel transmission scheme for the sake of linearly increasing the achievable throughput with the number of channels in an idealised crosstalk-free configuration.

Inspired by the concept of [93], numerous MIMO VLC system solutions were proposed in [94]–[100], [103], and [104]. Explicitly, in [104], the experimental demonstration of an indoor VLC MIMO system relying on a 2-by-2 white LED transmitter and a 3-by-3 receiver was presented, which operated at 2 [Mbps]. A substantially higher-speed 1 [Gbps] VLC MIMO system was demonstrated in [94], albeit its BER was as high as 10^{-3}. In [95], the MIMO receiver was improved with the aid of a hemispherical lens, which improved both the FOV and the receiver diversity gain. As a further substantial development, a multi-user transmit precoding assisted MIMO system was presented in [96], where the multi-user interference was eliminated by this transmit precoding scheme. The system operated at a data rate of 100 [Mbps] and a BER level of 10^{-6}. The associated resource allocation problems were first considered in the context of a VLC MIMO system in [97]. In [98], the BER performance analysis of diverse VLC MIMOs was studied, including both spatial diversity which mapped the same signal to several LEDs, using the above-mentioned concept of repetition coding and spatial multiplexing. The theoretical results were also confirmed by simulations. Again, a 2-by-2 LED VLC MIMO scheme relying on an image receiver[1] was also considered in [99], where a frequency

[1]Compared to the conventional MIMO receiver, the image receiver exploits a lens above the PDs to enhance difference of the the MIMO channels.

TABLE 3. A brief summary of contributions on indoor VLC MIMO techniques.

Year	Authors	Contributions
2009	L. Zeng [93]	Proposed a MIMO scheme relying on an image receiver for enhancing they system throughput
2013	A. H. Azhar *et al.* [94]	Constituted an MIMO-OFDM scheme on operating at 1 [Gbps] at a BER level of 10^{-3}
2013	T. Q. Wang *et al.* [95]	Employed a hemispherical lens in an indoor VLC MIMO arrangement for improving both FOV and the diversity gain
2013	Y. Hong *et al.* [96]	Proposed a multi-user transmit precoding aided MIMO system operating at 100 [Mbps] and a BER of 10^{-6}
2013	K.-H. Park *et al.* [97]	Conceived sophisticated resource allocation for indoor VLC MIMO
2013	T. Fath *et al.* [98]	Analysed the BER performance of indoor VLC MIMO schemes, including repetition coded MIMO and spatial multiplexing
2014	Y. Wang *et al.* [99]	Employed frequency domain equalisation in a indoor MIMO system
2014	T. Chen *et al.* [100]	Employed an ultra-wide fisheye lens for indoor VLC MIMOs capable of near-omnidirectional reception
2015	M. Biagi *et al.* [101]	Proposed an orthogonal PPM-STBC scheme under a rate constraint

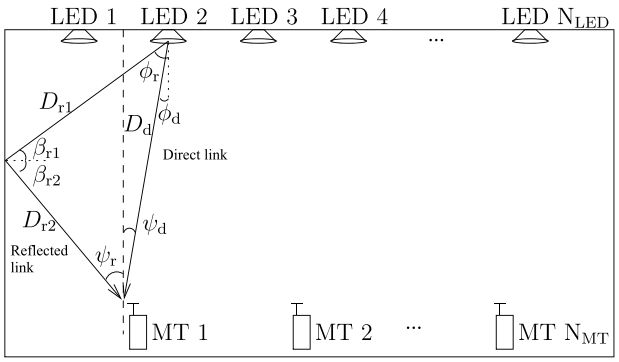

FIGURE 5. The 2D vertical axis-section of the room model in the VLC system.

domain equalisation method based on two pairs of time-multiplexed training symbols was proposed. Similar to [95], a novel fisheye lens was advocated in [100] for a VLC MIMO scheme relying on an image receiver, which achieved near-omnidirectional reception with the aid of an ultra-wide-angle fisheye lens. In [101], an orthogonal PPM-STBC scheme operating under specific rate constraints was proposed for VLC, while the authors of [102] investigated a suite of multi-user MIMO systems. We have summarised the indoor MIMO related studies in Table 3.

III. TRANSMISSION MODEL

A. 2D MULTIPLE LED MODEL

As mentioned in Section I, flawless power line communication is assumed to be used for linking up the LED transmitters. This idealized simplifying assumption will be eliminated in our future research. Having reviewed the background of indoor VLC systems, let us now consider the simplified model of a 2-Dimensional (2D) room having the length of 30 [m] and N_{LED} LED lights equi-distantly installed on the ceiling for serving N_{MT} MTs, as shown in Fig. 5, which

TABLE 4. System parameters of the indoor VLC system.

Room size and MTs' configuration	
Length of room	30 [m]
Height of room	3 [m]
Number of MTs N_{MT}	6
Height of MTs	0.85 [m]
Configuration of the VLC system	
Number of LEDs N_{LED}	8
Height of LEDs	2.5 [m]
Optical transmit power of LEDs $P_{\mathrm{t,o}}$	5.0, 7.0 [W]
semi-angle at half power $\Phi_{1/2}$	70°
Field-of-View Ψ_{c}	60°
Physical area of Detector on a PD A	1.0 [cm^2]
Gain of optical filter T_{s}	1.0
Refractive index of a lens at a PD n_{re}	1.5
Responsivity of a PD ξ	0.53 [A/W]
System modulation bandwidth B	1 [MHz]
Reflectance factor ρ	0.8
Electronic charge q	1.6×10^{-19} [C]
Boltzmann's constant κ	1.3806488×10^{-19}
Background current I_{bg}	5.1×10^{-3} [A]
Open-loop voltage gain G	10
Fixed capacitance of the PD per unit area η	1.12×10^{-6} [F]
FET channel noise factor Γ	1.5
FET transconductance g_m	3.0×10^{-2}
Noise bandwidth factor 1 I_{nb1}	0.562
Noise bandwidth factor 2 I_{nb2}	0.0868

are randomly distributed. In the following, we will introduce the channel model of this 2D room and further elaborate on a range of different transmission schemes in the context of this 2D model, as detailed in Table 4.

1) INDOOR CHANNEL MODEL

As demonstrated in Fig. 5, if we assume that ϕ_{d} is the angle of irradiation of the LED lights, ψ_{d} represents the angle of incidence, and D_{d} is the distance between a transmitter and a receiver. In an optical link, the channel's DC gain on directed path is characterised as [4]

$$H_{\mathrm{d}}(0) = \begin{cases} \dfrac{(l+1)\cos^{l}(\phi_{\mathrm{d}})A}{2\pi D_{\mathrm{d}}^2}\mathcal{G}_{\mathrm{d}}, & \text{if } \psi_{\mathrm{d}} \le \Psi_{\mathrm{c}}, \\ 0, & \text{if } \psi_{\mathrm{d}} > \Psi_{\mathrm{c}}, \end{cases} \quad (1)$$

where l is the Lambertian emission order, which is given by semi-angle $\Phi_{1/2}$ at half illumination of an LED as $l = -\log_2 \cos(\Phi_{1/2})$ [6]. Furthermore, A is the physical area of the PD and Ψ_c denotes the FOV at the receiver. Eq. (1) indicates that once the angle of irradiation of a receiver is higher than the FOV, the receiver's Line-of-Sight (LOS) would be blocked. We assume $\mathcal{G}_d = T_s g(\psi_d) \cos(\psi_d)$, where T_s is the gain of optical filter, $g(\psi_d)$ is the gain of an optical concentrator. If n_{re} represents the refractive index, the gain of the optical concentrator can be characterised as [4]:

$$g(\psi_d) = \begin{cases} \dfrac{n_{re}^2}{\sin^2(\Psi_d)}, & \text{if } \psi_d \le \Psi_c, \\ 0, & \text{if } \psi_d > \Psi_c. \end{cases} \tag{2}$$

Apart from the VLC LOS reception, the MTs may also receive the VLC reflected path owing to the wall. The received optical power is given by the channel's DC gain on the direct LOS path $H_d(0)$ and reflected path $H_r(0)$, which may be written as:

$$P_{r,o} = P_{t,o} H_d(0) + \int_{walls} P_{t,o} dH_r(0), \tag{3}$$

where $P_{t,o}$ and $P_{r,o}$ denote the transmitted and received optical power, respectively. The channel DC gain on the first reflection dH_r is given by [4]:

$$dH_r = \begin{cases} \dfrac{(l+1)\cos^l(\phi_r) A \rho}{2\pi^2 D_1^2 D_2^2} \mathcal{J} \mathcal{G}_r dA_{wall}, & \text{if } \psi_r \le \Psi_c, \\ 0, & \text{if } \psi_r > \Psi_c, \end{cases} \tag{4}$$

where D_{r1} is the distance between an LED light and a reflecting surface, D_{r2} denotes the distance between a reflective point and a MT receiver, ρ_f is the reflectance factor, whilst dA_{wall} is a small reflective area. Similarly, we let $\mathcal{G}_r = T_s g(\psi_r) \cos(\psi_r)$, where $g(\psi_r)$ could be calculated in the same way of Eq. (2). Furthermore, we assume that $\mathcal{J} = \cos(\beta_1)\cos(\beta_2)$, where β_1 and β_2 represent the angle of irradiance to a reflective point and the angle of irradiance to a MT's receiver, respectively.

The dominant noise contribution is assumed to be the shot noise due to ambient light from windows. We also take thermal noise into account. Hence, the Gaussian noise of the receiver filter's output having a total variance of σ^2 may be expressed as [4]:

$$\sigma^2 = \sigma_{shot}^2 + \sigma_{thermal}^2. \tag{5}$$

According to [4], the variance of shot noise σ_{shot}^2 may be formulated as:

$$\sigma_{shot}^2 = 2q\xi P_{r,o} B + 2q I_{bg} I_{nb1} B, \tag{6}$$

where q is the electronic charge, ξ is the detector's responsivity. B is the equivalent noise bandwidth and I_{bg} denotes the background current caused by the background light. Additionally, the thermal noise variance is given by [4]:

$$\sigma_{thermal}^2 = \frac{8\pi\kappa T_K}{G} \eta A I_{nb1} B^2 + \frac{16\pi^2 \kappa T_k \Gamma_{FET}}{g_{FET}} \eta^2 A^2 I_{nb2} B^3, \tag{7}$$

where κ is the Boltzmann's constant, T_K represents the absolute temperature, G is the open-loop voltage gain, η denotes the fixed capacitance of the PD per unit area, Γ is the FET transconductance. The noise bandwidth factors I_{nb1} and I_{nb2} are constant experimental values. Here, according to [4] and [6], we opt for their typical values, as shown in Table 4.

2) VLC ACHIEVABLE THROUGHPUT

Because the system is constituted by multiple independent attocells serving multiple MTs, the interference emanating from the adjacent attocells is inevitable and has to be taken into account. We define the Signal-to-Interference-plus-Noise-Ratio (SINR) γ as the total electronic power received from the desired signal source normalised by the scale of the electronic noise power in a bandwidth of B plus the total electronic power received from the destructive interference sources according to different schemes $\mathcal{I}_{sch}$.

Furthermore, we assume that the system employs ACO-OFDM [105]. As detailed in [106], when an ACO-OFDM scheme is introduced into our VLC system, the relationship between the elctronic transmit power and optical transmit power is defined as

$$P_{t,e} = \pi P_{t,o}^2. \tag{8}$$

Hence, we define the received electronic SINR γ as:

$$\gamma = \frac{P_{r,e}}{\sigma^2 + \mathcal{I}_{sch}} = \frac{\pi \left[\xi P_{t,o} \left(H_d(0) + \int_{wall} dH_r(0)\right)\right]^2}{\sigma^2 + \mathcal{I}_{sch}}. \tag{9}$$

According to [75], the maximum achievable rate of the ACO-OFDM system may be characterised by its channel capacity of [106]

$$C_{ACO} = \frac{B}{4} \log_2(1+\gamma). \tag{10}$$

This simple formulation is based on the assumption that the signal is Gaussian distributed and that ACO-OFDM only has a normalised effective throughput of 1/4, because it exploits the so-called Hermitian symmetry property for the sake of generating real and positive symbols. Below we will investigate three different transmission schemes: UFR, HFRFT and VT.

B. UNITY FREQUENCY REUSE

Let us commence our discourse from the most straightforward technique of constructing a VLC attocell, which is simply based on considering each individual LED light as an independent attocell, resulting into UFR. Then the total

number of attocells N_{cell} equals the total number of LED lights N_{LED} in this UFR transmission scheme. In this case, the ith MT suffers form the interference contributed by the power $P_{\text{t,o}}^{(c',i)}$ emanating from the other attocells, which is represented by $\mathcal{I}_{\text{UFR}} = \pi\xi^2 \sum_{c'\neq c, c\in[1,N_{\text{cell}}]} \left(P_{\text{t,o}}^{(c',i)} H^{(c',i)}\right)^2$, where c and c' denote the indices of the serving attocell and interfering attocell, respectively. As a result, the received SINR $\gamma_{\text{UFR}}^{(c,i)}$ of the ith MT served by the cth attocell using UFR transmission may be written as

$$\gamma_{\text{UFR}}^{(c,i)} = \frac{\pi\left(\xi P_{\text{t,o}}^{(c,i)} H^{(c,i)}\right)^2}{\sigma^2 + \mathcal{I}_{\text{UFR}}}, \tag{11}$$

where σ^2 is the total noise variance at the receiver obtained from Eq. (5), while $P_{\text{t,o}}^{(c,i)}$ represents the DL transmit power assigned to the ith MT from the cth attocell. In this scheme, each attocell may serve multiple MTs within its coverage using the time-division based round-robin scheme of [107].

Let $P_{\text{r,e}}^{(c,i)} = \pi\left(\xi P_{\text{t,o}}^{(c,i)} H^{(c,i)}\right)^2$ represent the received electronic power of the ith MT, based on Eq. (10). Then the instantaneous achievable rate of the ith MT can be formulated as

$$r_{\text{UFR}}^{(c,i)} = \frac{B}{4}\log_2\left[1 + \frac{P_{\text{r,e}}^{(c,i)}}{\sigma^2 + \mathcal{I}_{\text{UFR}}}\right]. \tag{12}$$

Additionally, consider the optical transmit power limitation of $P_{\text{t,o}}^{\min} \leq P_{\text{t,o}}^{(c,i)} \leq P_{\text{t,o}}^{\max}$, where $P_{\text{t,o}}^{\min}$ is a small value higher than 0.

C. HIGER FREQUENCY REUSE FACTOR BASED TRANSMISSION

Given the shortcomings of the UFR, the HFRFT scheme is capable of eliminating the interference by simply assigning a pair of orthogonal frequencies to the neighbouring two LED lights. This is possible, because only a limited frequency-range of the white LEDs is exploited for communications.[2] Explicitly, in this transmission scheme, each LED light still illuminates an individual attocell, hence, the total number of attocells remains the same as in the UFR case. However, in each attocell, only half of the frequency band can be used, which results into a frequency reuse factor of 2, hence the adjacent-cell interference can be mitigated and the SINR can be improved at the cell-edge. For odd indexed attocells, the interference of the ith MT imposed by the HFRFT scheme is characterised as $\mathcal{I}_{\text{HFRFT}} = \pi\xi^2 \sum_{c'\neq c, c'\in[1,3,\cdots]} \left(P_{\text{t,o}}^{(c',i)} H^{(c',i)}\right)^2$, where c and c' denote the indices of the serving attocell and the interfering attocells from the other odd numbered attocells. The corresponding instantaneous SINR $\gamma_{\text{HFRFT}}^{(c,i)}$ may be defined as

$$\gamma_{\text{HFRFT}}^{(c,i)} = \frac{\pi\left(\xi P_{\text{t,o}}^{(c,i)} H^{(c,i)}\right)^2}{\sigma^2/2 + \mathcal{I}_{\text{HFRFT}}}. \tag{13}$$

If we let $P_{\text{r,e}}^{(c,i)} = \pi\left(\xi P_{\text{t,o}}^{(c,i)} H^{(c,i)}\right)^2$, the instantaneous achievable rate of the ith a MT of the cth attocell may be written as

$$r_{\text{HFRFT}}^{(c,i)} = \frac{B}{8}\log_2\left[1 + \frac{P_{\text{r,e}}^{(c,i)}}{\sigma^2/2 + \mathcal{I}_{\text{HFRFT}}}\right]. \tag{14}$$

D. VECTORED TRANSMISSION

For the sake of reducing the size of the dead-zone in the UFR regime without sacrificing the bandwidth efficiency, we may opt for merging several neighbouring LED attocells into a virtual cell. In each virtual cell, we could employ more advanced transmission schemes. More specifically, we introduce the Zero-Forcing (ZF) based VT[3] regime into our VLC system for mitigating the mutual interference amongst the attocells within a virtual cell. Explicitly, we propose the VT-2 scheme,[4] where two neighbouring LED lights form a virtual cell and exploit ZF transmission in order to simultaneously serve two MTs as a pair. For the n_{p}th MT pair, we have $\mathcal{P}_{n_{\text{p}}}$. Then the definition of an attocell set is given by $\mathcal{C} = \left\{\mathbf{c}_{\text{v}}^{(1)}, \cdots, \mathbf{c}_{\text{v}}^{(c)}, \cdots, \mathbf{c}_{\text{v}}^{(N_{\text{cell}}/2)}\right\}$, where we assume having an even number of LED. More explicitly, as shown in Fig. 5, LED 1 and LED 2 form $\mathbf{c}_{\text{v}}^{(1)}$, LED 3 and LED 4 constitute $\mathbf{c}_{\text{v}}^{(2)}$, etc. Therefore, for the i_{si}th MT served by the cth virtual cell $\mathbf{c}_{\text{v}}^{(c)}$, the interference in our VT-2 scheme is mainly contributed by the power $P_{\text{t,o}}^{(c',i_{si})}$ leaking from the other neighbouring virtual cells, namely $\mathcal{I}_{\text{VT2}}^{(c',i_{si})} = \pi\xi^2 \sum_{c'\neq c, c'\in[1,N_{\text{cell}}/2]} \left(P_{\text{t,o}}^{(c',i_{si})} H^{(c',i_{si})}\right)^2$, where c and c' represent the indices of the serving virtual cell and the interfering virtual cells, respectively.

As mentioned above, the proposed VT-2 scheme is capable of supporting the pair of MTs $\mathcal{P}_{n_{\text{p}}}$ in a certain frequency band. These two MTs of this virtual cell constitute a (2×2)-element MIMO system, as shown in Fig. 6, where for the cth virtual cell $\mathbf{c}_{\text{v}}^{(c)}$, the MIMO channel matrix $\mathbf{H}^{(c,\mathcal{P}_{n_{\text{p}}})}$ can be written as the individual channels' DC gain between the two LEDs and the two MTs. Then, within this virtual cell, a precoding matrix $\mathbf{G}^{(c,\mathcal{P}_{n_{\text{p}}})}$ is constructed for the sake of eliminating the interference between the MTs in $\mathcal{P}_{n_{\text{p}}}$, where we have $\mathbf{H}^{(c,\mathcal{P}_{n_{\text{p}}})}\mathbf{G}^{(c,\mathcal{P}_{n_{\text{p}}})} = \mathbf{I}$ and $\mathbf{I}$ is an identity matrix. To satisfy this requirement, $\mathbf{G}^{(c,\mathcal{P}_{n_{\text{p}}})}$ may readily be obtained by the pseudo-inverse of the channel matrix $\mathbf{H}^{(c,\mathcal{P}_{n_{\text{p}}})}$,

[2]The FFR concept is not considered in this paper, since it would require prompt frequency switching for every MT during their movement, which would gravely degrade the users' experience [19].

[3]VT may be viewed as a specific example of the classic Transmission Precoding (TPC) of RF systems, with the slight difference that the VLC channel is typically non-dispersive.

[4]For the simplicity of demonstration without any loss of generality, we only consider the coordination of the neighbouring pair of LED lights. More involved VT schemes increase the complexity of the VT scheme.

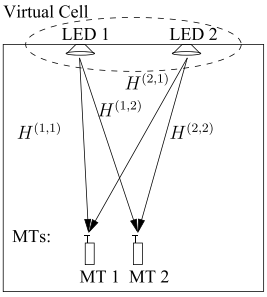

FIGURE 6. A simple illustration of VT-2 transmission in a virtual cell with multiple MTs.

which may be written as

$$\mathbf{G}^{(c,\mathcal{P}_{n_\mathrm{p}})} = \left(\mathbf{H}^{(c,\mathcal{P}_{n_\mathrm{p}})}\right)^{\mathrm{T}} \left[\mathbf{H}^{(c,\mathcal{P}_{n_\mathrm{p}})} \left(\mathbf{H}^{(c,\mathcal{P}_{n_\mathrm{p}})}\right)^{\mathrm{T}}\right]^{-1} = \begin{bmatrix} g_{1,1} & g_{1,2} \\ g_{1,2} & g_{2,2} \end{bmatrix}, \quad (15)$$

with $(\cdot)^{\mathrm{T}}$ denoting the transpose operation and $g_{c,i_{si}}$ representing the elements of the matrix. Then, if we let the signals transmitted from the LEDs within a virtual cell be represented by $\mathbf{x} = [x_1, x_2]^{\mathrm{T}}$, the received signals may be written as

$$\mathbf{y} = \mathbf{H}^{(c,\mathcal{P}_{n_\mathrm{p}})}\mathbf{G}^{(c,\mathcal{P}_{n_\mathrm{p}})}\mathbf{x} + \mathbf{v}, \quad (16)$$

where we have $\mathbf{v} = \left[v_{i_{s1}}, v_{i_{s2}}\right]^{\mathrm{T}}$, with each element denoting the noise imposed on the received signals, which have a variance given by Eq. (5). Thus, unlike in the UFR and HFRFT regimes, according to this scheme, the instantaneous SINR definition of MT i_{si} in the VT-2 scheme is given by

$$\gamma_{\mathrm{VT2}}^{(c,i_{si})} = \frac{\xi^2 P_{\mathrm{r,e}}^{(c,i_{si})}}{\sigma^2 + \mathcal{I}_{\mathrm{VT2}}^{(c,i_{si})}}, \quad (17)$$

where for each MT i_{si}, the received electronic power $P_{\mathrm{r,e}}^{(c,i_{si})} = \xi^2 P_{\mathrm{r_e,e}}^{(c,i_{si})}$ is contributed by the equivalent received electronic power $P_{\mathrm{r_e,e}}^{(c,i_{si})}$ multiplied by the responsivity ξ in a pair of LED lights within a virtual cell, and each LED light allocates only a commensurate fraction of optical power within its capability to serve a MT, while the rest of the power serves the other MT.

Since VT-2 does not partition its frequency resource, the instantaneous achievable rate is no longer halved, for MT i_{si} in virtual cell, its achievable rate can be expressed as

$$r_{\mathrm{VT2}}^{(c,i_{si})} = \frac{B}{4}\log_2\left[1 + \frac{P_{\mathrm{r,e}}^{(c,i_{si})}}{\sigma^2 + \mathcal{I}_{\mathrm{VT2}}^{(c,i_{si})}}\right]. \quad (18)$$

MT Scheduling: In this 2D VLC model, if the number of MTs is higher than the number of LED arrays in a virtual cell, then the order in which each MT is served has to be carefully determined, since the MT pairing process is of prime importance. Hence, we propose a two-stage MT pairing algorithm for finding beneficial pairing combinations of MTs, where the serving order of each pair is based on their channel conditions. Here, we have to point out that the MT pairing algorithm we proposed does not involve any specific power allocation based on Eq. (17). Instead, the power assigned to each light in the virtual cell remains the same. More explicitly, the two-stage MT pairing algorithm can be summarised as follows:

- *Cell Association Stage:* In this stage, each MT estimates the distance with respect to all LED lights, for example with the aid of an indoor positioning system and builds up the link to the nearest LED light, which results in the MT becoming associated with the virtual cell.
- *Search Stage:* In this stage, the MTs within the virtual cell are divided into different pairs for the sake of exploiting the VT-2 regime. After exhaustively searching all possible pairing combinations with the goal of maximising the sum of the achievable rate, we then obtain the best pairs and their serving orders in a virtual cell.

To be more specific, in the search stage, we assume that there is always an even number of MTs in a virtual cell. The search stage is formally detailed in Table 5.

TABLE 5. Search-Algorithm for MT pairing.

```
Searching:
For c_v^(c) ∈ C
    Find the MTs in its coverage
    Determine the number of serving MTs
    List all possible sorting combination
    For each sorting combination
        For for each MT pair
            Sum the achievable rate of MTs pairs Eq. (18)
        end
        Recoded the sum rate for this sorting combination
    end
    Find the best sorting pattern with the highest sum rate
end
Output: The sorted best MTs pairs in orders for all virtual cell
```

IV. VIDEO STREAMING OPTIMISATION

Historical Overview of Video Compression

Uncompressed video sequences captured from a real-world scene exhibit a high correlation amongst pixels. Intuitively, the correlation residing in an uncompressed video sequence should be removed in order to represent the uncompressed video with the aid of less bits, yet without any substantial loss of the perceived visual quality. Video compression will reduce the size of storage in a hard-drive for example, or the transmission bandwidth and the transmission power required for distributing the video. Hence, a number of video compression standards [21] have been designed during the past decades, such as H.120, H.261, H.263, which have found diverse applications, as exemplified in [22] and [23], followed by the more recent H.264/AVC and MPEG-4 standards designed for the sake of achieving a high compression ratio.

A. BRIEF HISTORY OF VIDEO COMPRESSION [112]

The timeline of the video coding standards is shown in Fig 7. The first video recorder was invented as early as in the 1950s,

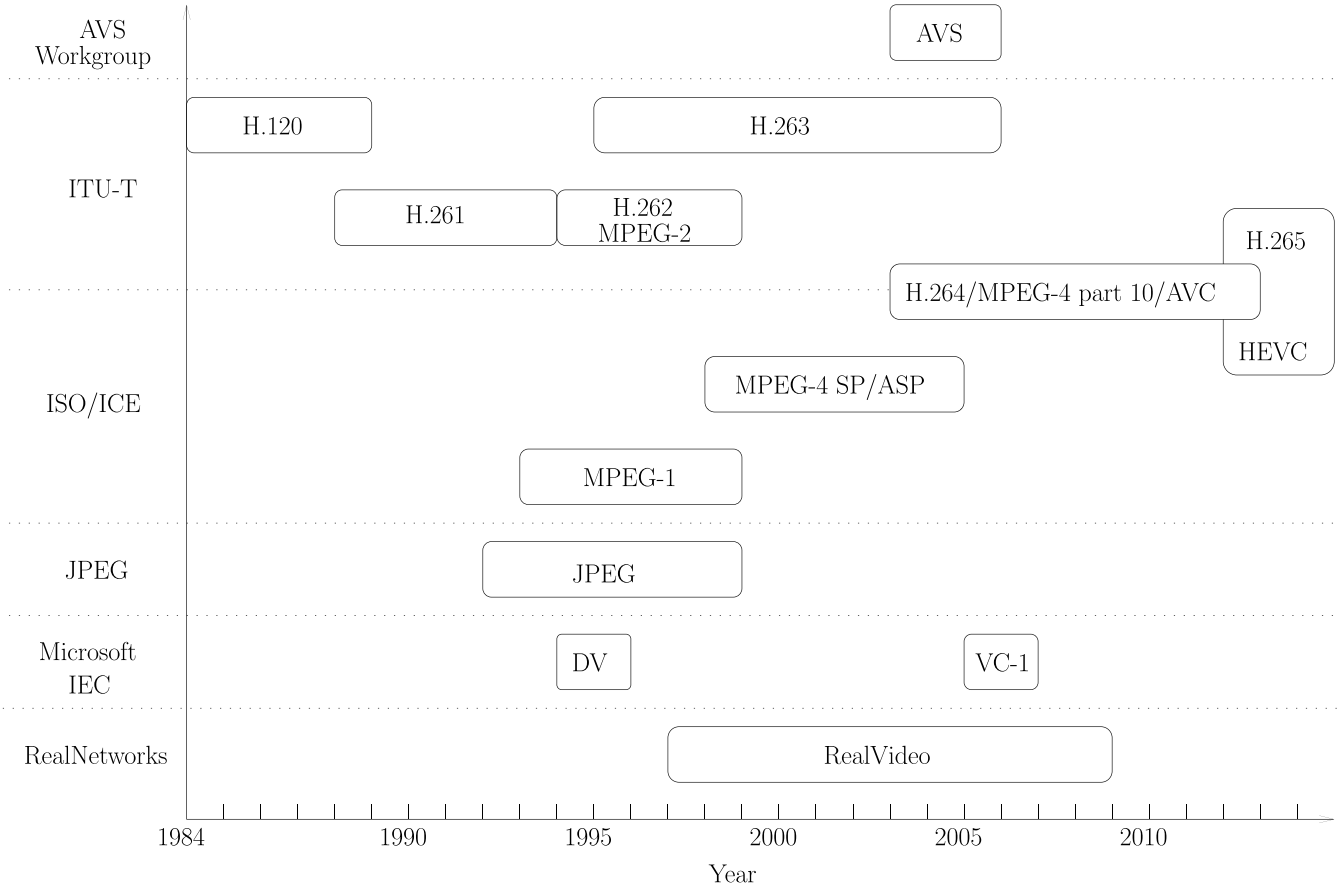

FIGURE 7. **Timeline of the video compression standards [112].**

but facilitated by the advances both in sophisticated digital signal processing algorithms and their implementations obeying Moore's law, video communications has been attracting intense research attention since the 1980s, as seen at a glance in Table 6.

For more details on video compression and video communications please refer to [21], where numerous application examples have been provided in the context of video streaming over the operational second-, third and fourth-generation RF wireless systems, whilst the benefits of multiuser MIMO-aided RF solutions were documented in [39].

However, as evidenced by Figure 2, the popularity of wireless video communications has resulted in a spectrum-crunch, which may be conveniently mitigated with the aid of the VLC solutions conceived in this treatise. Having said this, despite the plausible benefits of opting for VLC-based video streaming, apart from a few recent examples [40]–[43], there is a paucity of VLC-based video streaming solutions, which inspired our research.

Having briefly reviewed the history of video compression and communication, let us now focus our attention on the video traffic generated by the video codec employed in our multiuser VLC-based video investigations.

B. VIDEO TRAFFIC MODEL

Let us first discuss the basic traffic model and the principle of our video optimisation. We construct a system supporting a total of N_{MT} MTs, where each MT aims for downloading a pre-encoded video stream over an independent link. For simplicity, all MTs request the same video streams. In a video stream, the video frames are encoded on a Group-of-Pictures (GOPs) basis, by the video codecs, e.g. the H.264 [108] and H.265 [109] schemes. Within each GOP structure, the video frames are encoded using motion estimation inter-dependently. Each video frame within a GOP can be of Intra-frame (I) Type, Bidirectional (B) Type or Predicted (P) type, as detailed in [21]. The dependency of the intra-GOP video frames is shown in Fig. 8.

In this example, the GOP structure is IBBPBBP, where the I type video frame is independent of any other video frames, which is hence the most important one in a GOP. By contrast, the P type video frame depends on the preceding I and P video frames. Finally, the B type video frame is dependent on both the preceding and succeeding I or P video frames. Hence the following B and P type video frames will be affected, if the I video frame is corrupted.

For the simplicity of exposition and without any loss of generality, in this treatise, we assume an N_{F}-video frame

TABLE 6. Video history at a glance [112].

H.120 (1984-1988)	The International Telecommunication Union (ITU) standardized the first ever digital video compression standard known as H.120 [24], which relied on low-complexity differential pulse code modulation and hence was only capable of modest compression. This resulted in a relatively high bitrate, which limited its practical employment in the low-rate channels of this embrionic era of digital communications.
H.261 (1988-1993)	The ITU's H.261 standard [21], [25] of the 1990s, was conceived for transmitting both 352×288-pixel Common Intermediate Format [25] (CIF) and 176×144-pixel Quarter Common Intermediate Format [25] (QCIF) video clips over Integrated Services Digital Networks (ISDN). The first one in a sequence of CIF/QCIF video frames was a so-called intra-frame coded picture, which was followed by say 10 or so inter-frame coded pictures, where the latter exploited the similarity of the consecutive frames with the aid of motion compensation. More explicitly, each inter-frame coded CIF/QCIF frame was partitioned into perfectly tiling (8 x 8)-pixel blocks. Each of these blocks was then compared to a carefully selected search area surrounding the corresponding (8 x 8)-pixel block in the previous intra-coded picture and then it was subtracted from the most similar block of this so-called motion-compensation search area. The resultant motion-compensated error residual (MCER) was then transformed to the spatial frequency domain with the aid of the Discrete Cosine Transform (DCT), because the correlated (8 x 8)-pixel blocks typically resulted in a low number of low-frequency DCT coefficients, which hence required a lower number of quantization bits than the original MCER samples generated after motion compensation. This successful encoding philosophy has been adopted by literally all video encoding standards of the past few decades.
Joint Photographic Experts Group (1992-1998+)	Motion-JPEG standard emerged from the Joint Photographic Experts Group [26] (JPEG), which was originally formed for digital still image compression and hence encoded a video clip as a sequence of independent JPEG-compressed images, ie. as a sequence of intra-coded pictures. Whilst the motion-compensation used by the H.261 codec is prone to error propagation across the consecutive frames, this is not the case for the JPEG codec, but the price for its error resilience is its higher bitrate, ie lower compression ratio. This solution has been used by proprietary digital cameras and video processing systems, but it has not been standardized.
MPEG-1 (1993-1998+)	The Moving Picture Experts Group (MPEG) developed the MPEG-1 standard in 1992 [27] for CIF videos in parallel to the ITU's H.261 codec, with predominantly video storage and broadcast applications in mind, rather than lip-synchronized low-delay teleconferencing applications.
MPEG-2/H.262 (1994-1998+)	In 1993, the ITU and MPEG joined forces and in a concerted effort, they developed the MPEG-2/H.262 [29] standard for (720×576)- or (720×480)-pixel resolutions, and for high-definition (HD) video with a pixel resolution of 1920×1080. At the time of writing MPEG-2 is widely used as the format of digital TeleVision (TV) signals, which are broadcast by terrestrial, cable and direct satellite TV systems.
DV (1994-1995+)	The Digital Video (DV) coding specification of [30] was standardized by the International Electrotechnical Commission (IEC) in 1994, mainly targeting camera recorders, which encodes a video clip on a frame-by-frame basis, i.e. by dispensing with motion compensation. The DV efficiency is comparable to that of the Intra-frame (I) coding mode of MPEG-2/H.262, but it is better than that of Motion-JPEG.
H.263 (1995-2005)	The H.263 specification was standardized in 1995 by the ITU Telecommunication Standardization Sector [31] (ITU-T), which targeted video conferencing at low bitrates for mobile wireless communications and it is superior to all prior standards in terms of its compression efficiency. The H.263v2 standard, namely H.263+, was completed in 1998, which is the informal acronym for the second edition of the ITU-T H.263, which enhanced the H.263 capabilities by adding several annexes for substantially improving the encoding efficiency. Later, the definition of H.263v3, also known as H.263++, added three further annexes in 2000.
RealVideo (1997-2008+)	RealVideo [32] is a successful proprietary video compression format developed by the RealNetworks company, which was first released in 1997. RealVideo is supported by numerous computing platforms, including Windows, Mac, Linux, Solaris and several mobile phones.
MPEG-4 SP/ASP (1998-2004+)	MPEG-4 standardization [21] was initiated in 1995 and has been continually enhanced by a number of new profiles, including wavelet-based still image coding, scalable coding, 3D images etc. The MPEG-4 video standard strikes an adjustable quality versus bitrate trade-off, where the so-called Simple Profile (SP) is very similar to H.263, while the Advanced Simple Profile (ASP) further increased the compression efficiency attained.
WMV9/VC-1/SMPTE 421M (2005-2006+)	The society of Motion Picture and Television Engineers (SMPTE) 421M [33] developed a scheme, which is, also known as Windows Media Video version 9 (WMV9). This was initially developed as a proprietary video format by Microsoft, but it was then released as a SMPTE video codec standard in 2006. VC-1 was designed as an alternative to the latest ITU-T and MPEG video codec H.264/MPEG-4 AVC. It was shown that the VC-1 compression efficiency is lower than that of H.264, while imposing a reduced computational complexity.
H.264/MPEG-4 part 10/AVC (2003-2012)	The H.264 standard [34], also known as MPEG-4 part 10 or Advanced Video Coding (AVC), was completed in May 2003, albeit its research continued by adding more extentions. H.264/MPEG-4 part 10/AVC was jointly developed by the ITU-T Video Coding Experts Group (VCEG) and the ISO/IEC JTC1 MPEG, which became one of the most commonly used formats of video recording, compression and distribution. The design goal was to halve the bitrate required by the previous video standards, while retaining the same video quality. A major recent extension of H.264 was the Scalable Video Coding [35] (SVC) scheme completed in 2007, which is specified in Annex G, allowing the construction of bitstreams that contain sub-bitstreams of the H.264 standard. Another major extension of H.264 was the Multiview Video Coding scheme (MVC) completed in 2009 [36], which is specified in Annex H, enabling the construction of bitstreams that represent more than one view of a video scene. The MVC extension contains two profiles, which are the Multiview High Profile [34] representing an arbitrary number of views and the Stereo High Profile [34] for stereoscopic video.
Audio and Video Coding Standard (2003-2005)	The Advanced Video Standard (AVS) [37] was initiated by the government of China for replacing MPEG-2, which has been standardized in 2005. The AVS coding efficiency is comparable to that of the H.264/AVC scheme, which is achieved at a lower computational complexity.
HEVC/MPEG-H Part 2/H.265 (2012-2013+)	High Efficiency Video Coding (HEVC) [38] is undergoing development as a successor to H.264/AVC, which is being jointly developed by the ISO/IEC MPEG and ITU-T VCEG as ISO/IEC 23008-2 MPEG-H Part 2 and ITU-T H.265. HEVC aims for halving the bitrate of the H.264/AVC standard at the same video quality and it aims for supporting Ultra High Definition (UHD) videos at a resolution of 8192×4320. The emerging H.265 will continue to support SVC, which has not been widely adopted by the industry at the time of writing. For more details on video compression and video communications please refer to [21], where numerous application examples have been provided in the context of video streaming over the operational second-, third and fourth-generation RF wireless systems, whilst the benefits of multiuser MIMO-aided RF solutions were documented in [39].

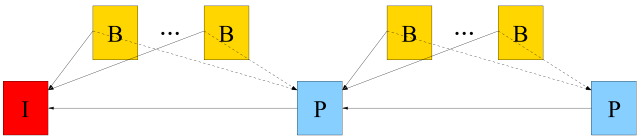

FIGURE 8. Structure of video frames in a GOP, where we use the IBBPBBP video frame structure. The dependency among the intra-GOP video frames is represented by arrows.

video stream relying on the same GOP structure for each MT. Let the set of video frames in a GOP downloaded by the ith MT be denoted by $\mathcal{F}_{\mathrm{GOP}}^{(i)} = \left\{f^{(i,1)}, \cdots, f^{(i,j)}, \cdots, f^{(i,N_{\mathrm{F}})}\right\}$, where $f^{(i,j)}$ represents the jth video frame in the ith MT's GOP. Furthermore, due to the different content of each video frame in the video stream, we assume that the rate required for transmitting this video frame $f^{(i,j)}$ is $r_{\mathrm{req}}^{(i,j)}$, where we define the video frames' required rate as the number of bits in the video frame over the time interval between consecutive video frames. Let $\gamma_{\mathrm{P}}^{(i,j)}$ denote the PSNR of the video frame $f^{(i,j)}$. To be more explicit, before its transmission the video stream is compressed by the video codec. The PSNR of each video frame represents the logarithmic Mean Square Error (MSE) between the original video frame and the compressed video frame in [dB].

We assume that in our model, we let an estimation window include n_{f} video frames $\mathcal{F}^{(i)} = \left\{f^{(i,1)}, \cdots f^{(i,n_{\mathrm{f}})}\right\}$ stored in a buffer before the transmission. Based on the knowledge of CSI among different MTs, the video frames are first scheduled and then assigned the appropriate transmit power. Consequently the achievable VLC rate of each MT is calculated, which is higher than the required rate of transmitting all the video frames in this window. As a result, before each MT is served, each transmitter will choose the best set of video frames to be transmitted and to be discarded. By employing 'frame copy' scheme, every discarded video frame will be directly replaced by the previous video frame.

We then denote the reconstructed window of the ith MT by $\mathcal{F}'^{(i)} = \left\{f'^{(i,1)} \cdots f'^{(i,n_{\mathrm{f}})}\right\}$ at the receiver. Considering the sophisticated bit allocation of a video clip, we hence invoke a relatively simple model for our simulation in this paper, namely that a frame dropping event only affects the dropped video frame itself without any inter-frame error propagation. Naturally, due to the differences between the above-mentioned pair of models having a difference is inevitable. However, we will demonstrate the rationale of invoking our simplified model in the following discussions.

For the ith MT, we let $\boldsymbol{\theta}^{(i)} = \left\{\theta^{(i,1)}, \cdots, \theta^{(i,j)}, \cdots, \theta^{(\mathrm{i},\mathrm{n_f})}\right\}$, which indicates the video frames' transmission status. Explicitly, $\theta^{(i,j)}$ characterises the status of each video frame, where $\theta^{(i,j)} = 0$ represents transmitting and $\theta^{(\mathrm{i},\mathrm{j})} = 1$ represents discarding a video frame. Then the total distortion experienced by the ith MT is simply the sum of the single-video-frame distortion's expressed in terms of PSNR, which is written as

$$\mathcal{D}^{(i)}\left(\boldsymbol{\theta}^{(i)}\right) = \sum_{j=1}^{n_{\mathrm{f}}} \Delta^{(i,j)}\theta^{(i,j)}, \tag{19}$$

where $\Delta^{(i,j)} = \gamma_{\mathrm{P}}^{(i,j)} - \gamma_{\mathrm{P}}^{\prime(i,j)}$, is a weighting factor that represents the PSNR difference between the original video frame $f^{(i,j)}$ and the recovered video frame $f'^{(i,j)}$. We also denote the video frame-status vector of the ith MT $\boldsymbol{\theta}^{(i)}$ as the ith row of the matrix $\boldsymbol{\theta}$, which includes the video frame status of all MTs. Additionally, owing to the specific GOP structure, we should consider the dependence relationship among the different types of video frames. Based on the features of the I and P video frames, when an I video frame is not scheduled for transmission, due to encountering an interference-contaminated links, the rest of the video frames in the GOP should will also be affected. As a consequence, the whole GOP is replaced by the most recently received one.

Given the scheduling-decision status of each video frame, the window size[5] required for transmitting the selected video frames of the ith MT is the total size of the ith original video frames $\sum_{j=1}^{n_{\mathrm{f}}} r_{\mathrm{req}}^{(i,j)}$ minus the total size of discarded video frames, which is the actual achieved video rate:

$$\mathcal{W}^{(i)}\left(\boldsymbol{\theta}^{(i)}\right) = \sum_{j=1}^{n_{\mathrm{f}}} r_{\mathrm{req}}^{(i,j)}\left(1 - \theta^{(i,j)}\right). \tag{20}$$

The system structure is shown in Fig. 9, the video stream is first stored in a long enough buffer. In the optimisation block, the algorithm determine transmit or discard the video frames based on the known Channel State Information (CSI). At receive side, the received date is then recovered to video stream.

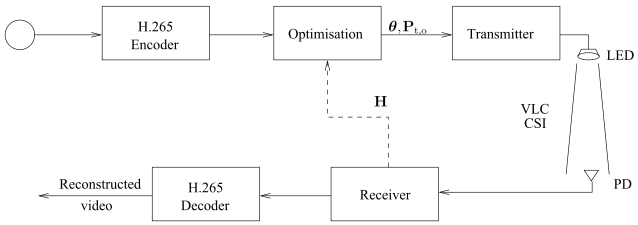

FIGURE 9. The structure of our video stream optimisation system.

C. OPTIMISATION PROBLEM FORMULATION

In a GOP, the video frames scheduling and power control is carried out individually for each MT based on the channel conditions and interference levels encountered on a frame-by-frame basis, where again only the selected video frames in a GOP are transmitted. The process of deciding about the most appropriate transmitted video frames can be solved as an optimisation problem, which is described below.

The objective of the optimisation problem is to minimise the total distortion of all video frames for all MT's video stream. For each MT, the optimisation problem is subject to the constraint that the total achievable VLC rate of a MT's transmission scheme could provide should be at least equal to the window size $\mathcal{W}^{(i)}\left(\boldsymbol{\theta}^{(i)}\right)$. The total achievable VLC rate available for the video frames in the entire video stream

[5]Here we define the required window size as the total number of bits representing all the frames in the estimation window.

is dominated by the instantaneous SINR γ, as we defined in Eq. (11), (13) and (17). Given the upper bound $P_{\mathrm{t,o}}^{\max}$ of the maximum transmit power and Eq. (8), the instantaneous SINR γ is a function of the received electronic power of each video frame $P_{\mathrm{r,e}}^{(c,i,j)}$. Furthermore, considering that the constraints imposed on the optical transmit power in different schemes are also different, we specifically elaborate on the problem in the UFR and HFRFT schemes, which can be deemed to be identical. On the other hand, the problem of the VT-2 scheme has to be described by a different problem.

1) PROBLEM FORMULATION FOR UFR AND HFRFT

Based on Eq. (19) and (20), we aim for minimising the total distortion of all video frames for each MT's video stream, as detailed in Eq. (21). Furthermore, for each MT, the achievable VLC rate defined in Eq. (20) should be higher than its total required video rate by a GOP, which is described by Eq. (22), based on the channel capacity detailed in Eq. (10). Additionally, the optical transmit power assigned to each video frame should also not exceed the maximum optical power constraint.

Based on these, the optimisation problem of the UFR and HFRFT schemes may be formulated as:

$$\text{Prob. 1}: \min_{\boldsymbol{\theta}^{(i)}} \sum_{i=1}^{N_{\mathrm{MT}}} \mathcal{D}^{(i)}\left(\boldsymbol{\theta}^{(i)}\right) \tag{21}$$

$$\text{s. t.}: \quad \mathcal{W}^{(i)}\left(\boldsymbol{\theta}^{(i)}\right) \leq \sum_{j=1}^{n_{\mathrm{f}}} B_{\mathrm{avb}} \log_2\left[1+\frac{P_{\mathrm{r,e}}^{(c,i,j)}(1-\theta^{(i,j)})}{\sigma_{\mathrm{sch}}^2+\mathcal{I}_{\mathrm{sch}}}\right], \quad \forall i \tag{22}$$

$$\text{var.s}: \quad 0 \leq P_{\mathrm{r,e}}^{(c,i,j)} \leq \pi\left(\xi H^{(c,i,j)} P_{\mathrm{t,o}}^{\max}\right)^2, \quad \forall i,j \tag{23}$$

$$\theta^{(i,j)} = \begin{cases} 0, & f^{(i,j)} \text{ transmitted}, \\ 1, & f^{(i,j)} \text{ discarded}, \end{cases} \tag{24}$$

where B_{avb} and σ_{sch}^2 represent the available system bandwidth and the noise variance of the different schemes, as detailed in Eq. (12) and (14). Explicitly, for a video clip associated with a scanning-rate of 30 Frame per Second (FPS), we have UFR: $B_{\mathrm{avb}} = \frac{B}{4\mathrm{FPS}}$, $\sigma_{\mathrm{sch}}^2 = \sigma^2$ and HFRFT: $B_{\mathrm{avb}} = \frac{B}{8\mathrm{FPS}}$, $\sigma_{\mathrm{sch}}^2 = \sigma^2/2$. Furthermore, we let $P_{\mathrm{r,e}}^{(c,i,j)}$ represent the received electronic power of the ith MT's jth video frame under the cth attocell, which is dominated by its corresponding optical transmit power $P_{\mathrm{t,o}}^{(c,i,j)}$. Furthermore, we let $H^{(c,i,j)}$ denote the channel DC gain of the jth video frame between the ith MT and the cth attocell. Finally, $\mathcal{I}_{\mathrm{sch}}$ is the total interference, where we consider the worst-case scheme that the interference received from the interfering cells is maximum, hence we have $\mathcal{I}_{\mathrm{sch}} = \pi\xi^2 \sum_{c'\neq c, c'\in[1,\cdots,N_{\mathrm{cell}}]} \left(P_{\mathrm{t,o}}^{\max} H^{(c',i,j)}\right)^2$ and $\mathcal{I}_{\mathrm{sch}} = \pi\xi^2 \sum_{c'\neq c, c'\in[1,3,\cdots]} \left(P_{\mathrm{t,o}}^{\max} H^{(c',i,j)}\right)^2$ for the UFR and HFRFT scheme, respectively, if we consider an odd-indexed attocell as an example.

2) PROBLEM FORMULATION FOR VT-2

Since the VT-2 scheme serves a pair of MTs simultaneously instead of a single one, the problem formulation is different from the above.

Explicitly, we will formulate the optimisation problem for the VT-2 scheme as listed in Eq. (25) - (28), as shown at the bottom of this page.

In Problem 2, we let n_{p} represent the index of the MT pairs, hence $\boldsymbol{\theta}^{(n_{\mathrm{p}},i_{si})}$ denotes the scheduling-decision based video frame status of the i_{si}th MT in the n_{p}th MT pair. Furthermore, $P_{\mathrm{r,e}}^{(c,n_{\mathrm{p}},i_{si},j)}$ is the i_{si}th MT's equivalent received electronic power of the jth video frame in the n_{p}th MT pair within the virtual cell $\mathbf{c}_{\mathrm{v}}^{(c)}$. Finally, $g_{c,i_{si}}^{(n_{\mathrm{p}},j)}$ denotes the specific element of the jth video frame's precoding matrix in the n_{p}th MT pair. We may notice that, since ZF TPC is used in the VT-2 scheme, the equivalent received electronic power of each MT is constrained by the elements of the precoding matrix $\mathbf{G}$ described in Eq. (15), which indicates that the power transmitted to each MT in a pair should not exceed the power limit of a LED light in an attocell.

V. NUMERICAL RESULTS AND DISCUSSIONS

In this section, considering the formulated problems are non-convex problems, we present our numerical results for

$$\text{Prob. 2}: \min_{\boldsymbol{\theta}^{(n_{\mathrm{p}},i_{si})}} \sum_{n_{\mathrm{p}}=1}^{N_{\mathrm{MT}}/2} \sum_{i_{si}=1}^{2} \mathcal{D}^{(n_{\mathrm{p}},i_{si})}\left(\boldsymbol{\theta}^{(n_{\mathrm{p}},i_{si})}\right) \tag{25}$$

$$\text{s. t.}: \quad \mathcal{W}^{(n_{\mathrm{p}},i_{si})}\left(\boldsymbol{\theta}^{(n_{\mathrm{p}},i_{si})}\right) \leq \sum_{j=1}^{n_{\mathrm{f}}} \frac{B}{4\mathrm{FPS}} \log_2\left[1+\frac{\xi^2\left(1-\theta^{(n_{\mathrm{p}},i_{si},j)}\right)P_{\mathrm{r,e}}^{(c,n_{\mathrm{p}},i_{si},j)}}{\sigma^2+\mathcal{I}_{\mathrm{VT2}}^{(c,n_{\mathrm{p}},i_{si})}}\right], \quad \forall n_{\mathrm{p}} \tag{26}$$

$$\text{var.s}: \begin{cases} \frac{1}{\sqrt{\pi}}\sqrt{\left(g_{1,1}^{(n_{\mathrm{p}},j)}\right)^2 P_{\mathrm{r,e}}^{(c,n_{\mathrm{p}},i_{\mathrm{s}1},j)} + \left(g_{1,2}^{(n_{\mathrm{p}},j)}\right)^2 P_{\mathrm{r,e}}^{(c,n_{\mathrm{p}},i_{\mathrm{s}2},j)}} \leq P_{\mathrm{t,o}}^{\max}, \quad \forall n_{\mathrm{p}}, j \\ \frac{1}{\sqrt{\pi}}\sqrt{\left(g_{2,1}^{(n_{\mathrm{p}},j)}\right)^2 P_{\mathrm{r,e}}^{(c,n_{\mathrm{p}},i_{\mathrm{s}1},j)} + \left(g_{2,2}^{(n_{\mathrm{p}},j)}\right)^2 P_{\mathrm{r,e}}^{(c,n_{\mathrm{p}},i_{\mathrm{s}2},j)}} \leq P_{\mathrm{t,o}}^{\max}, \quad \forall n_{\mathrm{p}}, j \end{cases} \tag{27}$$

$$\theta^{(n_{\mathrm{p}},i_{si},j)} = \begin{cases} 0, & f^{(n_{\mathrm{p}},i_{si},j)} \text{ transmitted}, \\ 1, & f^{(n_{\mathrm{p}},i_{si},j)} \text{ discarded}. \end{cases} \tag{28}$$

characterising the proposed problem using the Nonlinear Optimisation by Mesh Adaptive Direct Search (NOMAD) algorithm of [110] in the context of our indoor VLC video transmission system. More specifically, we mainly consider the following pair of transmission schemes:

- *Fixed Position Based Scenario:* we fix the position of a MT and investigate its PSNR degradation for characterising the performance attained at this specific location.
- *Random-Walk Based Scenario:* we allow the MTs to randomly move in the 2D room model. Then the Channel Impulse Response (CIR) experienced during each video frame of each MT becomes different, which are averaged in order to characterise the average performance across the room. These experiments are repeated 30 times for the sake of generating statistically relevant results.

Furthermore, in the different transmission schemes, the MTs are served in different order, depending whether the transmission scheme we considered involves a MT transmission scheduling scheme. Additionally, we assume that the channel conditions experienced by each user are identical during each of the different transmission schemes for the sake of fair performance comparisons among the three different transmission schemes, namely the UFR, the HFRFT and the VT-2. We transmit the widely-used 'Football' video test sequence scanned at 30 FPS constituted by a total of 8 GOPs, where the length of a GOP is 8 video frames. We used the H.265 video codec, while all other parameters used are listed in Table 7.

TABLE 7. Parameters used in our video streaming optimisation.

Parameters	Values
Room model configuration	2D, 30×3 [m^2]
No. of LED lights N_{LED}	8
No. of MTs N_{MT}	6
Estimation window length n_{f}	2,4,8,16
Transmission schemes	UFR, HFRFT, VT-2
Video clip	Football
GOP per MT	8
GOP length	8 video frames
Video frames' structure in a GOP	IPPPPPPP
FOV	60°
Video-frame-size	CIF 352×288
FPS	30
Video codec	H.265
Packet length	1000
ACO-OFDM length	512

A. VIDEO DISTORTION

1) PSNR DEGRADATION DISTRIBUTION

Let us first consider the video PSNR degradation of a particular MT moving in the room. Fig. 10 shows the average PSNR degradation of a MT downloading a 64-frame video clip at each position in the room. The maximum optical transmit power is $P_{\mathrm{t,o}}^{\max} = 5.0$ and 7.0 [W], FOV $= 60°$, while the estimation window length is $n_{\mathrm{f}} = 4$ video frame duration. The 'Football' video clip encoded by the H.265 codec associated with the length of 8 GOPs $\times$ 8 $=$ 64 video frames is transmitted to this MT at each position. The same experimental conditions will be used throughout our forthcoming investigations, unless state otherwise.

Explicitly, Fig. 10(b) demonstrates the exact PSNR degradation, while Fig. 10(a) displays the potential positions of this particular MT between a pair of points A and B. Here we have to mention that since the VT-2 scheme simultaneously serves a pair of MTs, we set the other MT at the fixed location marked by the black dot in Fig. 10(a) to pair with our moving MT for calculating the PSNR degradation. At each position, the MT will download the whole video clip constituted by

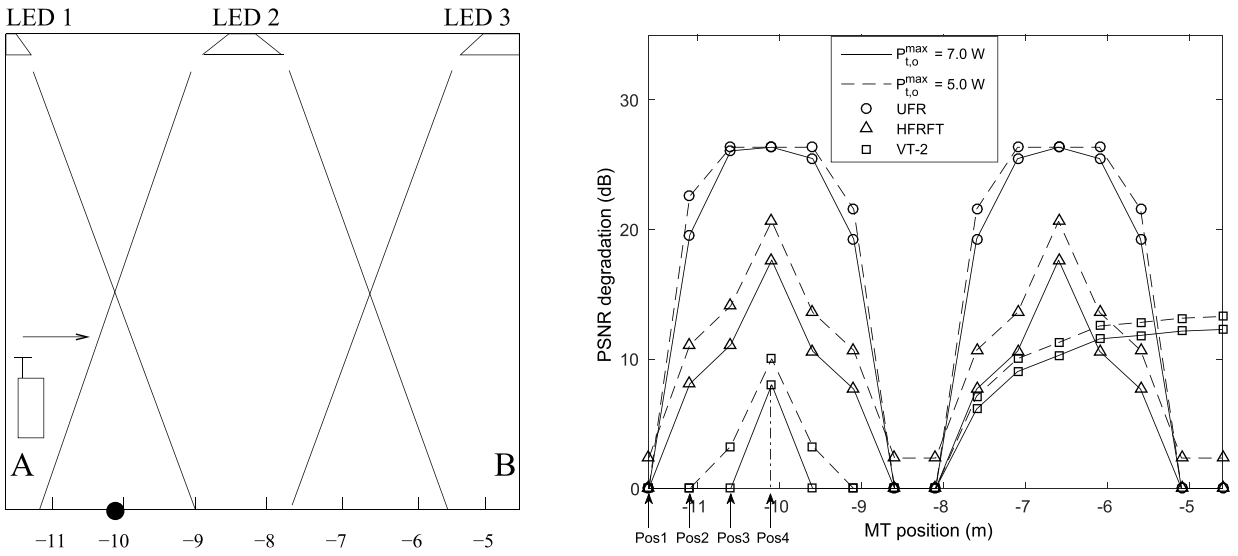

FIGURE 10. PSNR degradation vs. a single MT's position of the UFR, HFRFT and VT-2 schemes in the indoor VLC system of Fig. 5. The maximum optical transmit power is $P_{\mathrm{t,o}}^{\max} = 5.0$ and 7.0 [W]. The frame-by-frame performance degradation and the achievable video rate of the UFR, HFRFT and VT-2 schemes at Position 1 (−11.6 [m]), Position 2 (−11.1 [m]), Position 3 (−10.6 [m]) and Position 4 (−10.1 [m]) will be discussed in Fig. 11 - 14 and Fig. 17 - 20, respectively. The schematic of Fig. 9 and parameters in Table 7 are used.

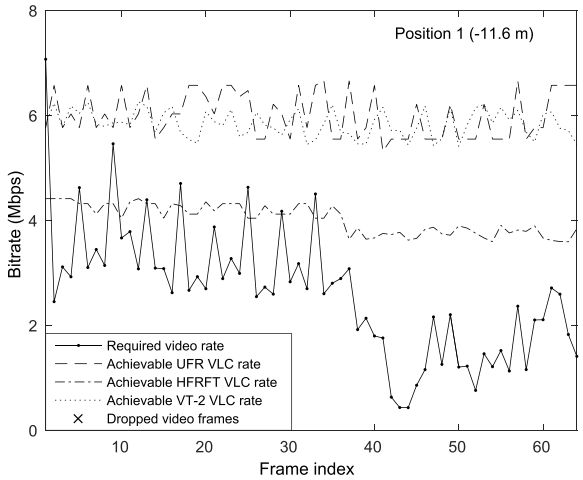

FIGURE 11. The required video rate before frame dropping (dotted solid line) and the achievable VLC rate of UFR, HFRFT and VT-2 in the indoor VLC system, when the MT is at Position 1 (−11.6 [m]) of Fig. 10(b). The maximum optical transmit power of $P_{t,o}^{max} = 7.0$ [W] is used. The curves represent the achievable VLC rate that system provided and the dropped-frames' indices are denoted by the markers. The schematic of Fig. 9 and the parameters of Table 7 are used. No video frames were dropped, hence no curve is seen for the x marker.

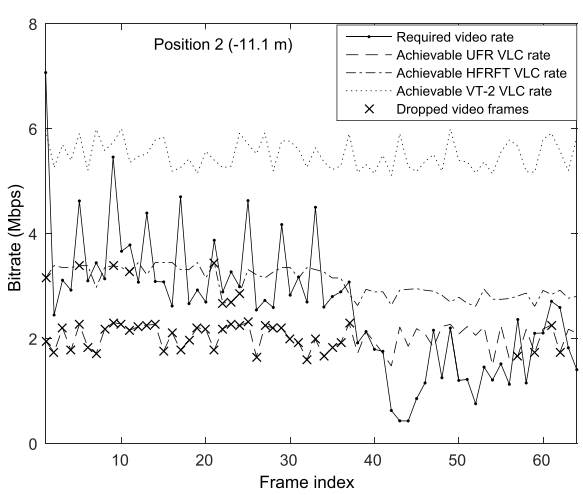

FIGURE 12. The required video rate before frame dropping (dotted solid line) and the achievable VLC rate of UFR, HFRFT and VT-2 in the indoor VLC system, when the MT is at Position 2 (−11.1 [m]) of Fig. 10(b). The maximum optical transmit power is $P_{t,o}^{max} = 7.0$ [W]. The curves represent the achievable VLC rate that the system provided and the dropped-frames' indices are denoted by the x markers. The schematic of Fig. 9 and the parameters of Table 7 are used.

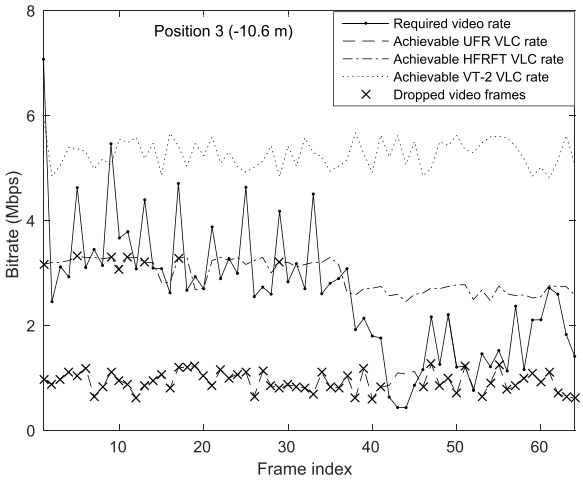

FIGURE 13. The required video rate before frame dropping (dotted solid line) and the achievable VLC rate of UFR, HFRFT and VT-2 in the indoor VLC system, when the MT is at Position 3 (−10.6 [m]) of Fig. 10(b). The maximum optical transmit power is $P_{t,o}^{max} = 7.0$ [W]. The curves represent the achievable VLC rate that system provided and the dropped-frames' indices are denoted by the x markers. The schematic of Fig. 9 and the parameters of Table 7 are used.

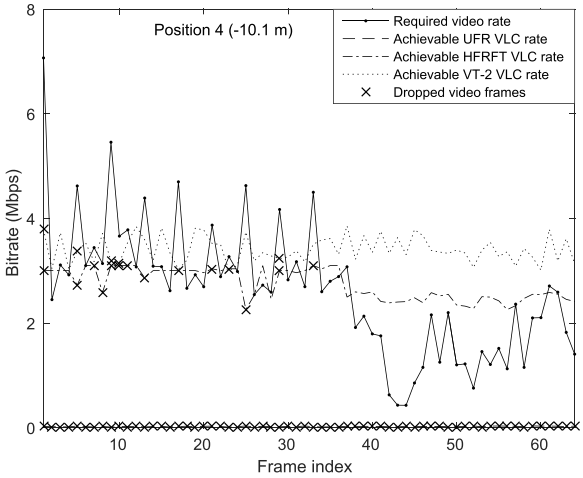

FIGURE 14. The required video rate before frame dropping (dotted solid line) and the achievable VLC rate of UFR, HFRFT and VT-2 in the indoor VLC system, when the MT is at Position 4 (−10.1 [m]) of Fig. 10(b). The maximum optical transmit power is $P_{t,o}^{max} = 7.0$ [W]. The curves represent the achievable VLC rate that system provided and the dropped-frames' indices are denoted by the x markers. The schematic of Fig. 9 and the parameters of Table 7 are used.

64 video frames under three different transmission schemes.

Let us first consider the PSNR degradation when we have $P_{t,o}^{max} = 7.0$ [W]. We observe that as expected, the PSNR degradation varies with the MT's position. More specifically, when the MT is right under the LED lights (−11.6 [m]), all three schemes provide a good PSNR performance, hence the PSNR degradation remains low. However, when the MT moves away from the LED lights, the performance degrades, especially when it is in the interference-contaminated area at Position 4 of Fig. 10(b) under the UFR scheme, when the video frames are discarded. This is because when the MT is exactly halfway between two LED lights, the MT suffers from the maximum amount of interference imposed by the adjacent attocell. In contrast to the UFR scheme, the PSNR degradation under the HFRFT scheme is much lower, because the adjacent attocells use non-interfering frequencies for the adjacent LED lights. Instead of being affected by the interfering power arriving from the neighbouring attocell, the PSNR degradation is now caused by the reduced interference as a benefit of having an increased distance from the interfering light source. Importantly, we observe that the VT-2 scheme

outperforms the other two schemes. The system only suffers from an approximately 8 [dB] PSNR degradation, when the MT is halfway between the two LED lights in a virtual cell. The reduced PSNR degradation is an explicit benefit of the VT-2 scheme jointly serving two MTs. However, when one of the paired MTs moves to −10.1 [m], its position almost overlaps with the paired MT denoted by the black dot in Fig. 10(a). Hence, their CIR becomes very similar and therefore their separation by the VT-2 scheme becomes imperfect. Furthermore, we have to mention that the PSNR degradation under the VT-2 scheme starts to increase more dramatically from the point onwards, when MT is at −8.1 [m]. This is because, the MT starts to suffer from the interfering power of LED 3. The PSNR degradation continues to increase, when the MT passed the −6.6 [m] position, because this MT is handed over to the virtual cell constructed by LED 3 and LED 4. If we still pair this MT with the MT at the fixed position of −10.6 [m], the system will no longer perform well. This is why the PSNR degradation keeps on increasing.

Additionally, if we reduce the maximum optical transmit power to $P_{\mathrm{t,o}}^{\max} = 5.0$ [W], as expected the system's performance degrades correspondingly, because only a lower power could be allocated to each video frame. Therefore, the PSNR degradation becomes more severe. Hence, in our following discussions, all the results are obtained for the system having the maximum transmit power of $P_{\mathrm{t,o}}^{\max} = 7.0$ [W].

2) FIXED POSITION BASED SCENARIO

Let us now explore the performance of VLC system under the UFR, HFRFT and VT-2 schemes. More explicitly, when the MT is at the four positions of −11.6, −11.1, −10.6 and −10.1 [m] in Fig. 10(a). We investigate the performance of these three schemes in Fig. 11 - 14, where the curves represent the achievable VLC rate of the system under our three schemes, while the markers exhibit the resultant video frame dropping events frame-by-frame. We may observe that the relative frequency of frame dropping events increases from Position 1 to 4, as shown in Fig. 11 to Fig. 14. This is mainly due to the degraded channel conditions explicitly portrayed in Fig. 10. More concretely, we may observe from Fig. 11 that both the UFR and VT-2 schemes are capable of providing a sufficiently high achievable VLC rate for satisfying the required video rate, when the MT is at Position 1. By contrast, the achievable HFRFT VLC rate is lower, but even then, no video-frames are dropped. This is because, we have to emphasise that according to the constraints of the optimisation detailed in Eq. (22) and Eq. (26), we evaluate the sum of the achievable VLC rate for all $n_{\mathrm{f}} = 4$ video frames, rather than that of every single video frame. Hence, even if the achievable VLC rate of the HFRFT scheme at a specific frame index is slightly lower than the required video rate, this is compensated by the lower required rate of the other video frames. As a result, the overall achievable VLC rate of all three scheme is sufficiently high. Therefore at Position 1, no video frames are dropped.

When the MT moves to Position 2, the performance of the three schemes is shown in Fig. 12. We may observe that compared to the performance at Position 1 of Fig. 12, the achievable VLC rate of the VT-2 scheme remains almost unchanged. By contrast, the achievable VLC rate of the HFRFT scheme is degraded, hence we can observe in the figure that some of the video frames are dropped, as indicated by the crosses at instances of having an increased required video rate. Finally, the achievable UFR VLC rate is dramatically reduced. Therefore, the sum of the achievable VLC rate is insufficient for transmitting all video frames. Hence, the optimisation algorithm tends to drop the specific video frames, which the system is unable to transmit. Explicitly, when the achievable VLC rate of the UFR scheme in an estimation window is lower than the required video rate of a specific video frame, but higher than the average required video rate, then the system may still be capable of transmitting the video frame, provided that some video-frames have a lower rate-requirement within this window. However, when the average video rate becomes higher than the achievable VLC rate, then some of the video frames have to be dropped. The indices of the dropped video frames are selected from the algorithm Table 8, which is constructed based on Eq. (22) and (26). When the achievable VLC rate experienced during a specific video frame is lower than the required video rate, but 'throughput deficit' is sufficiently low to be compensated during frame 38, this specific video frame is transmitted. By contrast, when the 'throughput deficit' is within the current optimisation window, as exemplified too high to be compensated by the rest of the frames in this optimisation window by the low rate of the future frames, as exemplified by frame 37, including the video frame will result in an overall achievable rate, which is lower than the sum of required video rates. Hence this video frame has to be dropped. As a result, observe in Fig. 12 that as many as 41 video frames of the UFR scheme are discarded.

To elaborate a little furhter, the performance of the three schemes at Position 3 is characterised in Fig. 13, where we may observe that the achievable VLC rate of the VT-2 scheme remains almost unchanged. By contrast, the achievable VLC rate of the UFR and HFRFT schemes is further degraded compared to their performance at Position 2 of Fig. 12, which is due to the further degraded channel condition, seen in Fig. 10(b). Then the achievable VLC rate of the UFR and HFRFT schemes is no longer capable of transmitting all the video frames at the Position 3 of Fig. 10(b). As a result, 8 video frames of the HFRFT scheme are discarded at this position. The most serious video degradation occurs in the UFR scheme, since almost all of the 64-video frames are dropped. The performance of the three schemes is further degraded, when the MT moves to Position 4 of Fig. 10(b), even that of the VT-2 scheme. Hence, even the VT-2 scheme starts to discard video frames. As we can see in Fig. 14, 5 video frames are dropped. In the UFR scheme the interference imposed by the adjacent attocell becomes as high as the derived signal itself. Hence, the achievable UFR VLC

TABLE 8. Video frame dropping algorithm.

Initialising:
$r_{\text{req}}^{(j)}$: required video rate of the jth video frame $r_{\text{vlc}}^{(j)}$: achievable VLC rate of the jth video frame
$R_{\text{sur}} = 0$: throughput surplus of video frames $\Delta_{\text{length}} = 0$: No. of pending frames
Δ_{index}: index of pending video frames
$\Delta_{\text{short}}^{(j)}$: throughput deficit of the jth pending video frame

If $\sum_{j=1}^{n_{\text{f}}} r_{\text{req}}^{(j)} \leq \sum_{j=1}^{n_{\text{f}}} r_{\text{vlc}}^{(j)}$
  For $j = 1 : n_{\text{f}}$
    If $r_{\text{vlc}}^{(j)} \to 0$
      $\theta^{(j)} = 1$ // dropped
    Otherwise
      $\theta^{(j)} = 0$ // transmitted
    End If
  End For
Otherwise If $\sum_{j=1}^{n_{\text{f}}} r_{\text{req}}^{(j)} > \sum_{j=1}^{n_{\text{f}}} r_{\text{vlc}}^{(j)}$
  For $j = 1 : n_{\text{f}}$
    If $r_{\text{req}}^{(j)} \leq r_{\text{vlc}}^{(j)}$
      $\theta^{(j)} = 0$ // transmitted
      $R_{\text{sur}} = R_{\text{sur}} + r_{\text{vlc}}^{(j)} - r_{\text{req}}^{(j)}$ // accumulate the throughput surplus
    Otherwise
    $\theta^{(j)} = 1$ // hold and buffered
      $\Delta_{\text{length}} = \Delta_{\text{length}} + 1$ // update the No. of pending video frames
      $\boldsymbol{\Delta}_{\text{index}}(\Delta_{\text{length}}) = j$ // update the index of pending video frames
      $\boldsymbol{\Delta}_{\text{short}}(\Delta_{\text{length}}) = r_{\text{req}}^{(j)} - r_{\text{vlc}}^{(j)}$ // update the throughput deficit
    End If
  End For
  $\left[\bar{\boldsymbol{\Delta}}_{\text{short}} \;\; \bar{\boldsymbol{\Delta}}_{\text{index}}\right] = \text{sort}(\boldsymbol{\Delta}_{\text{short}})$ // sort the throughput deficit ascendingly and record indices
  For $j = 1 : \Delta_{\text{length}}$ // check all hold and buffered video frames
    If $R_{\text{sur}} \geq \bar{\boldsymbol{\Delta}}_{\text{short}}^{(j)}$ // associated deficit of the jth video frame could be compensated
      $\theta^{(j)} = 0$ // transmit the video frame
      $R_{\text{sur}} = R_{\text{sur}} - \bar{\boldsymbol{\Delta}}_{\text{short}}^{(j)}$ // update the deficit
    Otherwise
      Terminate For Loop // drop the rest of video frames
    End If
  End For
End If

rate has been decreased to almost zero, therefore the system has to discard all the video frames. As a result, the PSNR degradation reaches its maximum of 26.35 [dB].

3) RANDOM-WALK SCENARIO

Based on characterising the performance of the four featured positions of Fig. 10(b) in the room, let us now continue by considering the PSNR degradation of a particular MT in a set of 6 MTs moving around in the room randomly. Fig. 15 shows the frame-by-frame video PSNR degradation of a MT, where the movement trajectories of the MT in the UFR, HFRFT and the VT-2 schemes are identical. At this stage, we have to clarify the differences between the two different video distortion models, as we mentioned in the Sec. IV-B, which is:

- *The Estimated Distortion Model:* The video distortion quantified in terms of the PSNR degradation is obtained from our optimisation results using the simplified video model mentioned in Sec. IV-B.
- *The Simulated Distortion Model:* Given the frame dropping indices extracted from the above estimated results, we can readily calculate the PSNR degradation caused by the dropped frames.

More explicitly, the dashed line marked by the dots represents the video distortion in terms of the PSNR for each frame of the video stream using the estimation-based distortion model over the time duration of a $8 - \text{GOP} = 8 \times 8 = 64$ video frame clip for our UFR, HFRFT and VT-2 transmission schemes. As seen in Fig. 15, the optimisation algorithm of Eq. (21) - (24) and Eq. (25) - (28) uses the parameters detailed in Table 7 for beneficially selecting the specific video frames, which may be discarded based on the constraints of Sec. V-C. By contrast, in practice, the dropped frames also affect the following video frames in a GOP. Hence, the solid line seen in Fig. 15 without markers portrays the resultant PSNR degradation of the video clip using the simulation-based distortion model of Sec. V-A3. A video frame dropped in the previous GOP does not affect the video quality in the current GOP. Observe in Fig. 15 that the more video frames are dropped, the higher the PSNR distortion of the video clip becomes. Explicitly, the PSNR degradation extracted from the estimation is seen to be lower than the simulated video distortion. However, both methods we used for estimating the PSNR degradation are reasonable, demonstrating similar trends for the UFR, HFRFT and VT-2 transmission schemes.

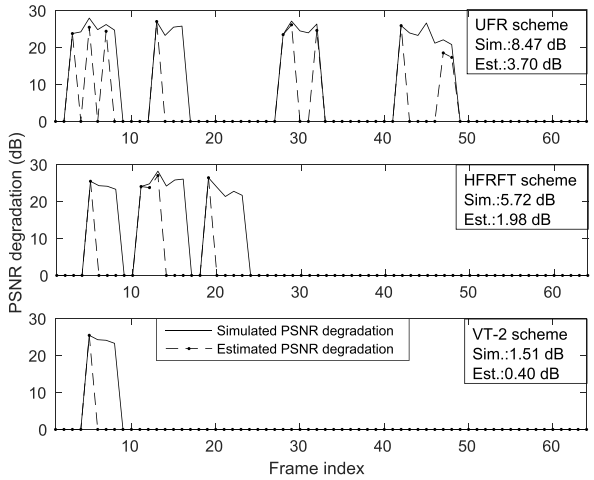

FIGURE 15. The PSNR degradation vs. video frame index for a single MT served by the UFR (top), HFRFT (middle) and VT-2 (bottom) schemes in the indoor VLC system of Fig. 5. The maximum optical transmit power is $P_{t,o}^{max} = 7.0$ [W]. The schematic of Fig. 9 and the parameters of Table 7 are used. In contrast to Fig. 11 - 14, where the MTs are stationary at Points 1 - 4, in this scheme the MTs move around randomly.

In conclusion, the PSNR degradations characterised in this chapter are adequately reflect the simulation-based video distortion.

We may observe in Fig. 15 that some video frames discarded in the VT-2 scheme such as the 5th video frame, are also discarded in the UFR and HFRFT scheme, because the inferior channel conditions experienced by the MT in the VT-2 scheme are also experienced in the UFR and HFRFT schemes. In this situation, the resultant achievable VLC rate is too low for the transmission of the frame in the estimation optimisation window as seen for Position 4 in Fig. 14. Furthermore, we may notice that some of the video frames that are dropped in the UFR scheme are retailed in the HFRFT and VT-2 scheme, as exemplified by video frames 28, 29 and 32. This is because these video frames were scheduled for transmission in low-SINR zone of Fig. 15 in the UFR scheme, whilst at the same position in the HFRFT and VT-2 schemes, the SINR still remains sufficiently high for transmitting this video frame. Similar trends are also observed for Positions 2 and 3 as shown in Fig. 12 and 13. By contrast, some video frames, such as the 11th and 12th video frames are dropped in the HFRFT scheme, while the corresponding video frames are transmitted in the UFR and VT-2 schemes. This is because the channel conditions at these positions guarantee a sufficiently high achievable VLC rate in the UFR and the VT-2 schemes. By contrast, although the achievable VLC rate of the HFRFT scheme at these positions is still relatively high, it remains insufficient for transmitting all the video frames of a specific estimation window, as exemplified by Position 1 in Fig. 11. More specifically, this situation occurs in the first half of the video clip, where the required video rate is consistently higher than in the second half. Moreover, we may observe that only a single video frame is discarded in the VT-2 scheme. Hence, the VT-2 scheme suffers from the lowest PSNR degradation and the discarded video frames have different indices compared to the other two schemes. This is because the VT-2 scheme jointly serves two MTs. Hence the video distortion is jointly affected by the channels of both MTs. Thus we may tentatively conclude that the VT-2 scheme has the best performance of the three in terms of mitigating the detrimental channel conditions. Based on Fig. 15, a simple example of the test video streaming of 'Football' after video frame dropping has been displayed in Fig. 16 for the UFR, HFRFT and VT-2 schemes, respectively. Observe with reference to tWhe Fig. 15 that the UFR scheme imposes a PSNR degradation of 25 [dB] for the 4th video frame, which is similar to the HFRFT scheme, but a degradation of 0 [dB] is experienced to the VT-2 regime. Similar observation can be made at the remaining frame indices.

B. THE VIDEO RATE ACHIEVED

1) THE VIDEO RATE ACHIEVED OF FIXED POSITION SCENARIO

Having discussed the PSNR degradation of a single MT, let us now investigate the attainable performance by investigating the achieved video rate of the three schemes at the four fixed positions seen in Fig. 10(b), which are portrayed in Fig. 17 - Fig. 20.

We may observe from Fig. 17 - 20 that the actual achieved video rate is gradually reduced, as the MT moves from Position 1 to Position 4, which corresponds to the results we have shown in Fig. 11 - 14. More specifically, the final achieved video rate of the three transmission schemes at Position 1 is displayed in Fig. 11. We can see that since all the 64-video frames are transmitted, the achieved video rate of the three schemes remains identical to the original required video rate. When the MT moves to Position 2, we may observe that due to the dropped video frames of the UFR scheme, its achieved video rate at the corresponding frame indices of Fig. 12 becomes zero. By contrast, the achieved video rate of both the HFRFT as well as of the VT-2 schemes still remains identical to the required video rate. When the MT moves to Position 3 and Position 4, we observe that the achieved video rates are reduced. For example, for the UFR scheme at Position 4, the achieved video rate becomes zero, since the video could not be recovered at the receiver.

2) THE VIDEO RATE ACHIEVED OF RANDOMLY MOVE SCENARIO

Having discussed the PSNR degradation and the achieved video rate of a single MT, let us now investigate the attainable performance from a multi-MT perspective by investigating the average performance of multiple MTs randomly moving in the room of Fig. 5. Fig. 21 portrays the average achieved rate of the reconstructed video for all the six MTs considered, where we calculate the average achieved rate of each video frame deducting the bit rate requirements of the dropped video frames after video frame discarding in all three schemes. The original bit rate of the video stream before frame-discarding is also represented by the circle markers.

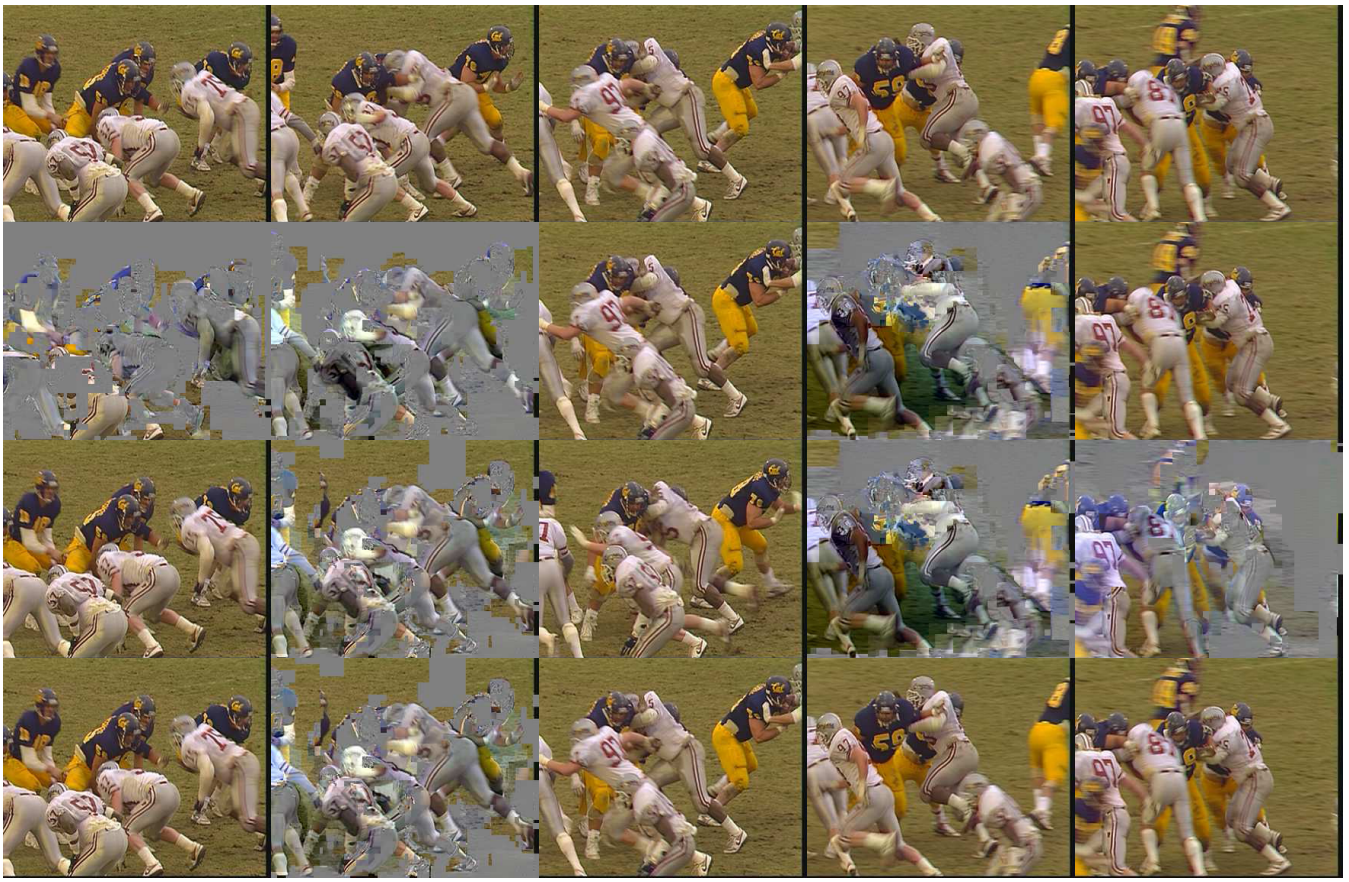

FIGURE 16. Five video frames of the 'Football' video test stream after video frame dropping, where the 4th, 8th, 12th, 16th and 20th video frames have been extracted from the original video stream (first row), UFR (second row), HFRFT (third row) and VT-2 (forth row) schemes, respectively. Observe with reference to the Fig. 15 that the UFR scheme imposes a PSNR degradation of 25 [dB] for the 4th video frame, which is similar to the HFRFT scheme, but a degradation of 0 [dB] is experienced to the VT-2 regime. Similar observation can be made at the remaining frame indices.

Observe that the VT-2 scheme achieves the highest rate in all three transmission schemes, especially the achieved video rate at all the I frames. By contrast, observe in Fig. 21 that the SINR of the I frames in the UFR and the HFRFT schemes is relatively low, while the VT-2 scheme is capable of preserving the I frames to avoid excessively video quality degradations. Hence, the VT-2 system is capable of providing high quality video coverage in the indoor environment considered.

C. PSNR DISTORTION VERSUS DELAY

Let us now characterise the effects of the estimation window length n_f, which indicates the number of video frames we store in the streaming buffer before their transmission. Hence, the window length directly determines the system delay. In other words, the longer the estimation window, the higher the system delay becomes. Given the video scanning-rate of FPS $=$ 30, in a delay sensitive system, we may opt for an estimation window length of $n_f = 4$, when the delay is $4/30 \approx 0.13$ seconds. However, if the system is capable of tolerating a longer streaming delay, we could employ a longer estimation window, such $n_f = 8$ and 16. Fig. 22 demonstrates the average PSNR degradation vs. the delay quantified in terms of the estimation window length

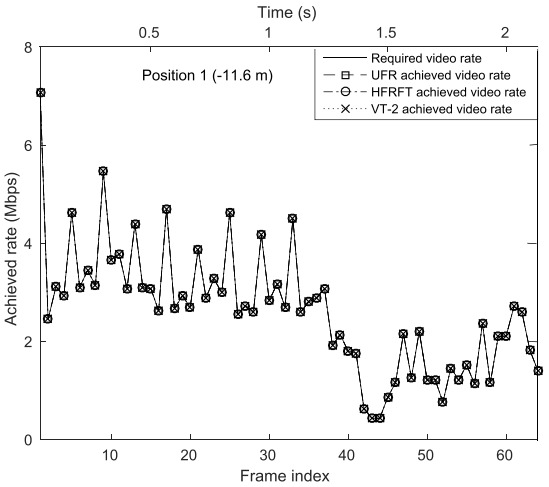

FIGURE 17. Achieved video rate vs. the video frame index of UFR, HFRFT and VT-2, when the MT is located at Position 1 (−11.6 [m]) of Fig. 10. The maximum optical transmit power is $P_{t,o}^{max} = 7.0$ [W]. The schematic of Fig. 9 and the parameters of Table 7 are used.

for all three different transmission schemes in our indoor VLC system. As expected, the average PSNR degradation is reduced for a longer estimation window. This is because a

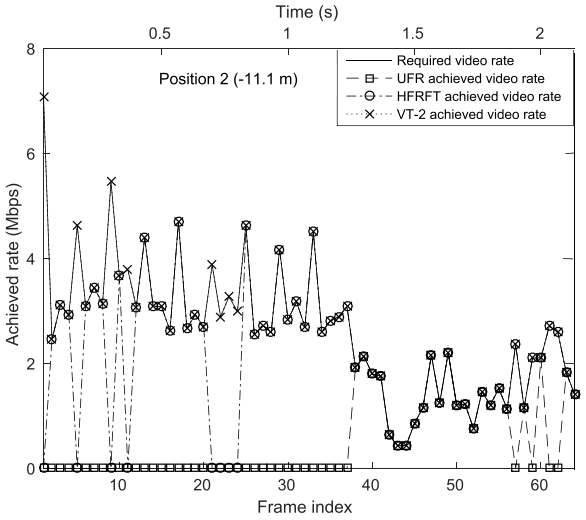

FIGURE 18. Achieved video rate vs. the video frame index of UFR, HFRFT and VT-2, when the MT is located at Position 2 (−11.1 [m]) of Fig. 10. The maximum optical transmit power is $P_{t,o}^{max} = 7.0$ [W]. The schematic of Fig. 9 and the parameters of Table 7 are used.

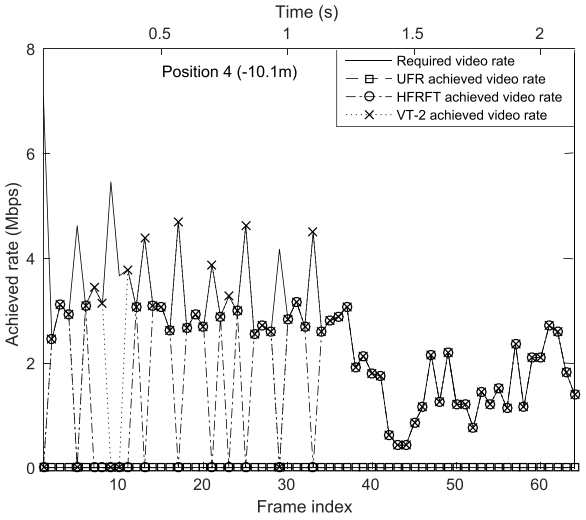

FIGURE 20. Achieved video rate vs. the video frame index of UFR, HFRFT and VT-2, when the MT is located at Position 4 (−10.1 [m]) of Fig. 10. The maximum optical transmit power is $P_{t,o}^{max} = 7.0$ [W]. The schematic of Fig. 9 and the parameters of Table 7 are used.

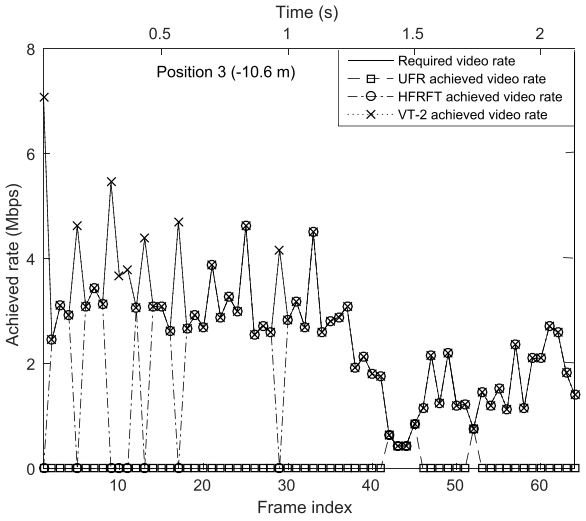

FIGURE 19. Achieved video rate vs. the video frame index of UFR, HFRFT and VT-2, when the MT is located at Position 3 (-10.6 [m]) of Fig. 10. The maximum optical transmit power is $P_{t,o}^{max} = 7.0$ [W]. The schematic of Fig. 9 and the parameters of Table 7 are used.

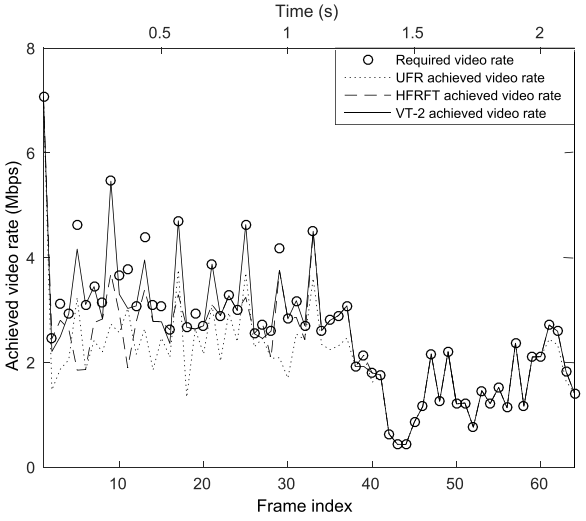

FIGURE 21. Average achieved rate of the system vs. the video frame index for all 6 MTs served under the UFR, HFRFT and VT-2 schemes in the indoor VLC system of Fig. 5. The maximum optical transmit power is $P_{t,o}^{max} = 7.0$ [W]. The schematic of Fig. 9 and the parameters of Table 7 are used.

longer estimation window allows the system to buffer and hence average the required rate of more video frames at specific channel conditions. Hence, if the achievable VLC rate associated with a specific video frame is lower than the required video rate, this may still be compensated as a benefit of having a longer estimation window and vice versa. Furthermore, for longer estimation window lengths, the PSNR degradation difference among the schemes is also reduced. More specifically, when the estimation window length equals $n_f = 2$, the PSNR degradation difference among the UFR, HFRFT and VT-2 regimes is approximately 8 [dB]. However, when the window length is increased to $n_f = 16$, the difference becomes as low as 3 [dB]. This implies that for longer estimation windows the performance of the UFR and the HFRFT schemes might be able to approach the performance of the VT-2 scheme more closely at the cost of a longer system delay, which is suitable for non-real-time broadcasting, but not for lip-synchronised multimedia teleconferencing.

D. OVERALL STATISTICS

Based on the results we have shown in Fig. 10 to Fig. 21, let us conclude with the evaluation of the average PSNR degradation, of the achievable rate and of the consumed energy in Fig. 23 using randomly move scheme. Based on the discussions on a specific MT, overall, the UFR scheme suffers

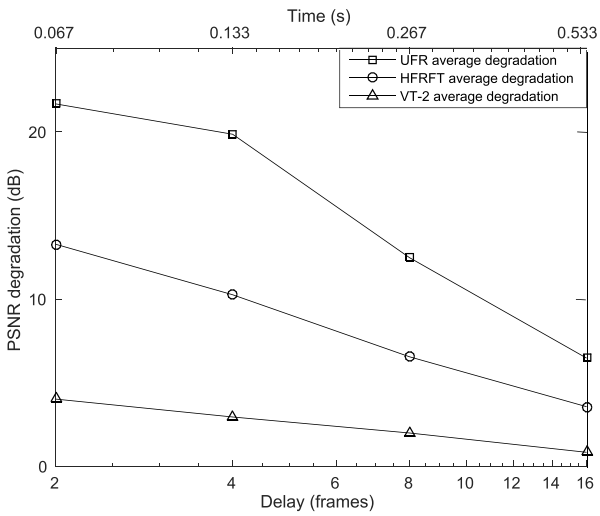

FIGURE 22. The average PSNR degradation vs. the delay in terms of the estimation window length of $n_f = 2$, 4, 8 and 16 averaged for all 6 MTs randomly moving in the room, served under the UFR, HFRFT and VT-2 schemes in the indoor VLC system of Fig. 5. The maximum optical transmit power is $P_{t,o}^{max} = 7.0$ [W]. The schematic of Fig. 9 and the parameters of Table 7 are used.

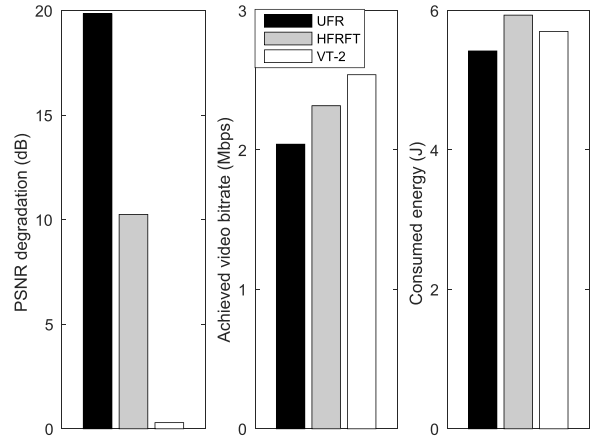

FIGURE 23. The average PSNR degradation (left), the achieved rate of the reconstructed video (middle) and the consumed energy (right) averaged for all 6 MTs served under the UFR (black), HFRFT (gray) and VT-2 (white) schemes in the indoor VLC system of Fig. 5. The maximum optical transmit power is $P_{t,o}^{max} = 7.0$ [W]. The schematic of Fig. 9 and the parameters of Table 7 are used.

from the highest PSNR degradation, the HFRFT scheme is slightly lower than that of the UFR scheme. However, both of these schemes are outperformed by the VT-2 scheme. In terms of the average achievable rate, we observe the same trends. Explicitly, the VT-2 scheme has the highest performance of the three. Recall from Fig. 21, the average achieved rate is almost 95% of that regime by the original video clip. By contrast, the achieved video rate of the UFR and of the HFRFT schemes is lower, but the latter performs better. In all of these results, we may observe that the VT-2 scheme has the best performance at the similar energy level to that of the HFRFT scheme. This implies that the VT-2 scheme intellectually allocates the transmit power and hence achieves an excellent PSNR performance.

VI. CONCLUSIONS, DESIGN GUIDELINES AND FUTURE RESEARCH

A. CONCLUSIONS

A novel video streaming optimisation framework was conceived for efficient video delivery in our VLC system. The attainable performance of the UFR, HFRFT and VT-2 schemes was compared in terms of their PSNR degradation, energy consumption, system delay and achievable rate. We first characterised the attainable performance of the MT at fixed positions in order to gain physically tangible insights into the effects of the associated propagation phenomena on the video quality degradations. Then we proceeded to quantify the average performance of the randomly moving MTs. Based on these studies we concluded that the proposed indoor VLC system is indeed capable of supporting high-quality multimedia transmissions, and that as expected, the VT-2 scheme provided a significantly better performance than the UFR and HFRFT schemes.

B. DESIGN GUIDELINES

We improved the overall quality of VLC-based video streaming systems by striking a compelling trade-off amongst the conflicting design constrains of PSNR degradation, video rate, system delay, energy dissipation and so on, as the basic motivation of our designs. Our investigations led to the design guidelines listed below:

- Based on the characteristics of our indoor model, we conceived and investigated the UFR, HFRFT and VT-2 regimes. Given its excellent performance in all the scenarios investigated, the VT-2 scheme is recommended.
- Naturally, it is futile to transmit at an excessive video rate, which exceeds the maximum VLC-rate that may be supported at any specific location of the atto-cells. If no channel-quality-controlled feedback is available for instructing the video codec to reduce its encoding rate, it is recommended that the system should resort to video-frame dropping.
- We note however that in delay-tolerant video broadcast scenarios, where longer buffering delays are tolerable, the fluctuation of the available VLC-rate may be counteracted by storing encoded video frames, until the tolerable video delay expires or until a buffer-overload is encountered. These findings indicate the presence of an explicit video quality versus delay trade-off, which has to be born in mind, when designing VLC-based video-streaming systems relying on the VT-2-based multi-user scenario.

C. FUTURE RESEARCH

A base-line VLC-aided video-streaming system was designed and investigated, which led to a range of design guidelines. Indeed, the transmission of high-resolution video streams has also been demonstrated in an indoor laboratory environment, as seen in Fig 24. Nonetheless, there are numerous open

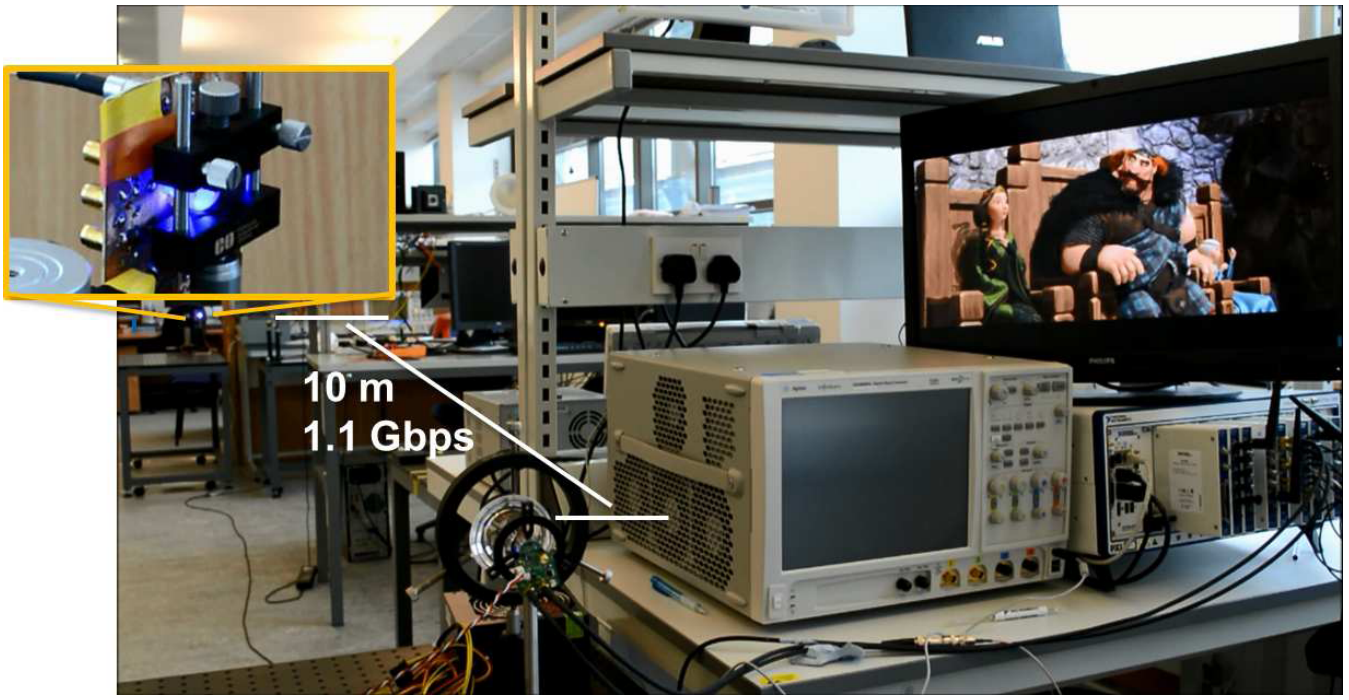

FIGURE 24. Demonstration of 1.1 Gbps VLC-aided video transmission system over a distance of 10m. The VLC transmitter is seen in magnified format at the top-left corner, which transmits the video signal to the receiver situated at the bottom of the picture. The received video picture is seen at the top-right corner.

problems to be solved by the research community, some of which are listed briefly below:

- In this early study of VLC-aided video-streaming a low-complexity buffer-assisted video-frame dropping regime was designed for accommodating the location-dependent channel quality of the atto-cells. However, given the location-dependent channel-quality fluctuation across the atto-cells, more sophisticated adaptive modulation and coding may be invoked for accommodating these channel-quality variations [21]–[23].
- Naturally, adaptive modulation and coding results in a location- and SINR-dependent bitrate constraint, which can be fed back to the video encoder for commensurately adjusting the video-rate for ensuring flawless error-free video delivery, as detailed in the classic RF context in [21]–[23] and [111]. [21]–[23], [111]. A particularly attractive solution is constituted by the employment of multi-layer video compression [112]– [116], where the most important base-layer is transmitted all the time to provide a basic low-resolution video service, whilst the additional enhancement-layers are transmitted in instances of high channel quality for the sake of improving the video quality.
- Sophisticated low-delay automatic repeat request (ARQ) [117], [118] schemes may also be designed for retransmitting the error-infested video frames.
- *All in all, an exciting era for VLC research!*

APPENDIX: LIST OF SYMBOLS

β_1	Irradiance angle to a reflected point.
β_2	Irradiance angle to the receiver.
γ	SINR.
γ_{P}	PSNR of the original video frame.
γ'_{P}	PSNR of the reconstructed video frame.
γ_{HFRFT}	SINR of the HFRFT scheme.
γ_{UFR}	SINR of the UFR scheme.
γ_{VT2}	SINR of the VT-2 scheme.
Γ_{FET}	The FET channel noise factor.
$\Delta^{(i,j)}$	The jth PSNR degradation of the ith MT.
η	Fixed capacitance of the PD per unit area.
κ	The Boltzmann's constant.
ϕ_{d}	Irradiance angle of the direct link.
ϕ_{d}	Irradiance angle of the direct link.
$\Phi_{\frac{1}{2}}$	The semi-angle at half illumination power.
ψ_{d}	Incidence angle of the direct link.
ψ_{r}	Incidence angle of the reflected link.
Ψ_{c}	FOV.
ρ	Reflectance factor.
θ	Video frame transmitter status.
$\boldsymbol{\theta}^{(i)}$	The ith video frame transmitter status vector.
ξ	The responsivity of the PD.
σ^2	The total noise variance.
σ^2_{shot}	The shot noise variance.
$\sigma^2_{\mathrm{thermal}}$	The thermal noise variance.
A	The physical area of the PD at receiver.
A_{wall}	The physical area of the reflected point.

B	Bandwidth.
B_{avb}	Available bandwidth of different scheme.
$\mathbf{c}_{\text{v}}$	Virtual cell.
C_{ACO}	Throughput of ACO-OFDM modulation.
$\mathcal{C}$	Transmission cells.
D_{d}	Physical distance of the LOS link.
D_1	Distance from the LED to the reflected point.
D_2	Distance from the reflected point to the PD.
$\mathcal{D}$	Total distortion of a MT's video stream.
$f^{(i,j)}$	The jth video frame of the ith MT.
$f'^{(i,j)}$	Recovered the jth video frame of the ith MT.
$\mathcal{F}$	Set of video frames.
$\mathbf{g}$	The gain of optical concentrator.
$\mathbf{G}$	Pseudo-inverse of channel matrix.
H_{d}	Channel DC gain of the LOS link.
H_{r}	Channel DC gain of the reflected link.
$\mathbf{H}$	MIMO channel matrix.
I_{bg}	Background current.
I_{nb}	Noise bandwidth factor.
$\mathcal{I}$	Interference.
$\mathcal{I}_{\text{sch}}$	Interference of different schemes.
$\mathcal{I}_{\text{UFR}}$	Interference of UFR scheme.
$\mathcal{I}_{\text{HFRFT}}$	Interference of HFRFT scheme.
$\mathcal{I}_{\text{VT2}}$	Interference of VT-2 scheme.
n_{f}	Length of the estimation window.
N_{cell}	Number of cells.
$N_{\text{LED}}]$	Numer of LEDs.
$N_{\text{MT}}]$	Number of MTs.
$P_{\text{r,o}}^{\max}$	Maximum received optical power.
$P_{\text{r,e}}^{\max}$	Maximum received electronic power.
$P_{\text{r}_{\text{e}},\text{e}}$	Equivalent received electronic power.
$P_{\text{t,o}}^{\max}$	Maximum transmitted optical power.
$P_{\text{t,e}}^{\max}$	Maximum transmitted electronic power.
$\mathcal{P}_{n_{\text{p}}}$	The n_{p}th serving pair.
$\mathbf{P}_{\text{r,e}}$	Received electronic power matrix.
$\mathbf{P}_{\text{r,o}}$	Received optical power martix.
$\mathbf{P}_{\text{t,e}}$	Transmitted electronic power matrix.
$\mathbf{P}_{\text{t,o}}$	Transmitted optical power matrix.
q	The electronic charge.
r_{req}	Required video rate of a video frame.
r_{UFR}	Achievable VLC rate of UFR scheme.
r_{HFRFT}	Achievable VLC rate of HFRFT scheme.
r_{VT2}	Achievable VLC rate of VT-2 scheme.
$\mathcal{W}$	Total achieved video rate of a MT.
T_{K}	The absolute temperature.
T_{s}	The gain of optical filter.

REFERENCES

[1] L. Hanzo, H. Haas, S. Imre, D. O'Brien, M. Rupp, and L. Gyongyosi, "Wireless myths, realities, and futures: From 3G/4G to optical and quantum wireless," *Proc. IEEE*, vol. 100, pp. 1853–1888, May 2012.

[2] J. G. Andrews *et al.*, "What will 5G be?" *IEEE J. Sel. Areas Commun.*, vol. 32, no. 6, pp. 1065–1082, Jun. 2014.

[3] E. Dahlman *et al.*, "5G wireless access: Requirements and realization," *IEEE Commun. Mag.*, vol. 52, no. 12, pp. 42–47, Dec. 2014.

[4] T. Komine and M. Nakagawa, "Fundamental analysis for visible-light communication system using LED lights," *IEEE Trans. Consum. Electron.*, vol. 50, no. 1, pp. 100–107, Feb. 2004.

[5] J. Jiang, R. Zhang, and L. Hanzo, "Analysis and design of three-stage concatenated color-shift keying," *IEEE Trans. Veh. Technol.*, vol. 64, no. 11, pp. 5126–5136, Nov. 2015.

[6] J. M. Kahn and J. R. Barry, "Wireless infrared communication," *Proc. IEEE*, vol. 85, no. 2, pp. 265–289, Feb. 1997.

[7] D. Tsonev, S. Videv, and H. Haas, "Light fidelity (Li-Fi): Towards all-optical networking," *Proc. SPIE*, vol. 9007, pp. 900702-1–900702-10, Dec. 2013.

[8] H. Zhang, L.-L. Yang, and L. Hanzo, "Compressed impairment sensing assisted and interleaved-double-FFT aided modulation improves broadband power line communications subjected to asynchronous impulsive noise," *IEEE Access*, to be published.

[9] X. Li, R. Zhang, and L. Hanzo, "Cooperative load balancing in hybrid visible light communications and WiFi," *IEEE Trans. Commun.*, vol. 63, no. 4, pp. 1319–1329, Apr. 2015.

[10] "Cisco visual networking index: Global mobile data traffic forecast update 2014–2019," White Paper, Mar. 2015. [Online]. Available: http://www.cisco.com/c/en/us/solutions/collateral/service-provider/visual-networking-index-vni/white_paper_c11-520862.html

[11] (2015). *Visible Light Communication—VLC & PureVLC*. [Online]. Available: http://andy96877.blogspot.co.uk/p/visible-light-communication-vlc-is-data.html

[12] D. Jurca and P. Frossard, "Video packet selection and scheduling for multipath streaming," *IEEE Trans. Multimedia*, vol. 9, no. 3, pp. 629–641, Apr. 2007.

[13] P. Pahalawatta, R. Berry, T. Pappas, and A. Katsaggelos, "Content-aware resource allocation and packet scheduling for video transmission over wireless networks," *IEEE J. Sel. Areas Commun.*, vol. 25, no. 4, pp. 749–759, May 2007.

[14] Y. Li, Z. Li, M. Chiang, and A. R. Calderbank, "Content-aware distortion-fair video streaming in congested networks," *IEEE Trans. Multimedia*, vol. 11, no. 6, pp. 1182–1193, Oct. 2009.

[15] F. Fu and M. van der Schaar, "Structural solutions for dynamic scheduling in wireless multimedia transmission," *IEEE Trans. Circuits Syst. Video Technol.*, vol. 22, no. 5, pp. 727–739, May 2012.

[16] K. Pandi, A. Ghosh, D. Ghosal, and M. Chiang, "Content aware optimization for video delivery over WCDMA," *EURASIP J. Wireless Commun. Netw.*, vol. 2012, p. 217, Jul. 2012.

[17] M. van der Schaar and D. S. Turaga, "Cross-layer packetization and retransmission strategies for delay-sensitive wireless multimedia transmission," *IEEE Trans. Multimedia*, vol. 9, no. 1, pp. 185–197, Jan. 2007.

[18] M. Ismail, W. Zhuang, and S. Elhedhli, "Energy and content aware multi-homing video transmission in heterogeneous networks," *IEEE Trans. Wireless Commun.*, vol. 12, no. 7, pp. 3600–3610, Jul. 2013.

[19] C. Chen, N. Serafimovski, and H. Haas, "Fractional frequency reuse in optical wireless cellular networks," in *Proc. IEEE 24th Int. Symp. PIMRC*, London, U.K., Sep. 2013, pp. 3594–3598.

[20] C. Chen, D. Tsonev, and H. Haas, "Joint transmission in indoor visible light communication downlink cellular networks," in *Proc. IEEE Globecom Workshops*, Atlanta, GA, USA, Dec. 2013, pp. 1127–1132.

[21] L. Hanzo, P. Cherriman, and J. Streit, *Video Compression and Communications: From Basics to H.261, H.263, H.264, MPEG4 for DVB and HSDPA-Style Adaptive Turbo-Transceivers*. New York, NY, USA: Wiley, 2007.

[22] P. Cherriman and L. Hanzo, "Programmable H.263-based wireless video transceivers for interference-limited environments," *IEEE Trans. Circuits Syst. Video Technol.*, vol. 8, no. 3, pp. 275–286, Jun. 1998.

[23] P. Cherriman, T. Keller, and L. Hanzo, "Orthogonal frequency-division multiplex transmission of H.263 encoded video over highly frequency-selective wireless networks," *IEEE Trans. Circuits Syst. Video Technol.*, vol. 9, no. 5, pp. 701–712, Aug. 1999.

[24] *Codecs for Videoconferencing Using Primary Digital Group Transmission*, document ITU-T Rec. H.120, Nov. 1988.

[25] *Video Codec for Audiovisual Services at $p \times 384$ kbit/s*, document ITU-T Rec. H.261, Nov. 1988.

[26] G. K. Wallace, "The JPEG still picture compression standard," *Commun. ACM*, vol. 34, no. 4, pp. 30–44, 1991.

[27] *Information Technology—Coding of Moving Pictures and Associated Audio for Digital Storage Media at up to About 1,5 Mbit/s—Part 2: Video*, document ISO/IEC 11172-2, 1993.

[28] *Conventional Analogue Television Systems*, document ITU-T Rec. BT.470, Feb. 2005.

[29] *Information Technology—Generic Coding of Moving Pictures and Associated Audio Information: Video*, document ITU-T Rec. H.262, Feb. 2012.

[30] *Recording—Helical-Scan Digital Video Cassette Recording System Using 6,35 mm Magnetic Tape for Consumer Use (525-60, 625-50, 1125-60 and 1250-50 Systems)—Part 2: SD Format for 525-60 and 625-50 Systems*, document IEC 61834-2, Aug. 1998.

[31] *Video Coding for Low Bit Rate Communication*, document ITU-T Rec. H.263, Jan. 2005.

[32] *The History and Future of Real Networks*, Internet Video Mag., May 2011.

[33] *SMPTE VC-1 Receiving Industrywide Support*. [Online]. Available: http://www.microsoft.com/en-us/news/press/2006/apr06/04-24VC1PR.aspx

[34] *AVC: Advanced Video Coding for Generic Audiovisual Services*, document ITU-T Rec. H.264/ISO/IEC 14496-10, Joint Video Team (JVT) of ISO/IEC MPEG and ITU-T VCEG, Mar. 2010.

[35] H. Schwarz, D. Marpe, and T. Wiegand, "Overview of the scalable video coding extension of the H.264/AVC standard," *IEEE Trans. Circuits Syst. Video Technol.*, vol. 17, no. 9, pp. 1103–1120, Sep. 2007.

[36] Y. Chen, Y.-K. Wang, K. Ugur, M. M. Hannuksela, J. Lainema, and M. Gabbouj, "The emerging MVC standard for 3D video services," *EURASIP J. Adv. Signal Process.*, vol. 2009, Jan. 2009, Art. ID 8.

[37] *Audio and Video Coding Standard*, AVS Workgroup China, Jan. 2005.

[38] *High Efficiency Video Coding*, document ITU-T Rec. H.265, Apr. 2013.

[39] D. Bethanabhotla, G. Caire, and M. J. Neely. (2014). "Adaptive video streaming in MU-MIMO networks." [Online]. Available: http://arxiv.org/abs/1401.6476

[40] D. K. Son, E. Cho, I. Moon, Z. Ghassemlooy, S. Kim, and C. G. Lee, "Simultaneous transmission of audio and video signals using visible light communications," *EURASIP J. Wireless Commun. Netw.*, vol. 2013, p. 250, Oct. 2013.

[41] Y. He, L. Ding, Y. Gong, and Y. Wang, "Real-time audio & video transmission system based on visible light communication," *Opt. Photon. J.*, vol. 3, no. 2, pp. 153–157, Jun. 2013.

[42] L. C. Png, "A fully integrated audio, video, and data VLC transceiver system for smartphones and tablets," in *Proc. IEEE 17th Int. Symp. Consum. Electron. (ISCE)*, Jun. 2013, pp. 249–250.

[43] O. Bouchet *et al.*, "Visible-light communication system enabling 73 Mb/s data streaming," in *Proc. IEEE GLOBECOM Workshop*, Dec. 2010, pp. 1042–1046.

[44] D. K. Jackson, T. K. Buffaloe, and S. B. Leeb, "Fiat lux: A fluorescent lamp digital transceiver," *IEEE Trans. Ind. Appl.*, vol. 34, no. 3, pp. 625–630, May 1998.

[45] Y. Tanaka, S. Haruyama, and M. Nakagawa, "Wireless optical transmissions with white colored LED for wireless home links," in *Proc. 11th IEEE Int. Symp. Pers., Indoor Mobile Radio Commun.*, vol. 2. Sep. 2000, pp. 1325–1329.

[46] (2007). *Visible Light Communications Consortium*. [Online]. Available: http://www.vlcc.net/modules/xpage1/

[47] J. Grubor, S. Randel, K.-D. Langer, and J. W. Walewski, "Broadband information broadcasting using LED-based interior lighting," *IEEE J. Lightw. Technol.*, vol. 26, no. 24, pp. 3883–3892, Dec. 15, 2009.

[48] (2012). *Home Gigabit Access Project*. [Online]. Available: http://www.ict-omega.eu/

[49] Bourns College of Engineering. (2012). *Center for Ubiquitous Communication by Light*. [Online]. Available: http://www.uclight.ucr.edu/

[50] The Pennsylvania State University. (2012). *Center on Optical Wireless Applications*. [Online]. Available: http://cowa.psu.edu/

[51] Smart Lighting Engineering Research Center. (2008). *Synthesizing Light for the Benefit of Humanity*. [Online]. Available: http://www.bu.edu/smartlighting

[52] *IEEE Standard for Local and Metropolitan Area Networks—Part 15.7: Short-Range Wireless Optical Communication Using Visible Light*, IEEE Standard 802.15.7-2011 Sep. 2011.

[53] M. H. Crawford, "LEDs for solid-state lighting: Performance challenges and recent advances," *IEEE J. Sel. Topics Quantum Electron.*, vol. 15, no. 4, pp. 1028–1040, Jul./Aug. 2009.

[54] H. Elgala, R. Mesleh, and H. Haas, "Indoor broadcasting via white LEDs and OFDM," *IEEE Trans. Consum. Electron.*, vol. 55, no. 3, pp. 1127–1134, Aug. 2009.

[55] R. Mesleh, H. Elgala, and H. Haas, "LED nonlinearity mitigation techniques in optical wireless OFDM communication systems," *IEEE/OSA J. Opt. Commun. Netw.*, vol. 4, no. 11, pp. 865–875, Nov. 2012.

[56] C. W. Chow, C. H. Yeh, Y. F. Liu, and Y. Liu, "Improved modulation speed of LED visible light communication system integrated to main electricity network," *Electron. Lett.*, vol. 47, no. 15, pp. 867–868, Jul. 2011.

[57] H. Hecht, "Changing the lights: Are LEDs ready to become the market standard?" *Opt. Photon. News*, vol. 23, no. 3, pp. 44–50, 2012.

[58] Cree Inc. (2012). *Cree Sets New R&D Performance Record With 254 Lumen-Per-Watt Power LED*. [Online]. Available: http://www.cree.com/news-and-events/cree-news/press-releases/2012/april/120412-254-lumen-per-watt

[59] N. Kumar and N. Lourenco, "Led-based visible light communication system: A brief survey and investigation," *J. Eng. Appl. Sci.*, vol. 5, no. 4, pp. 269–307, 2010.

[60] D. A. Steigerwald *et al.*, "Illumination with solid state lighting technology," *IEEE J. Sel. Topics Quantum Electron.*, vol. 8, no. 2, pp. 310–320, Mar./Apr. 2002.

[61] OSRAM Opto Semiconductors. (2013). *Multi-Chip LED*. [Online]. Available: http://www.osram-os.com/osram-os/en/product-catalog/led-light-emitting-diodes/multi-chipled/index.jsp

[62] Konica Minolta. (2014). *OLED Lighting*. [Online]. Available: http://www.konicaminolta.com/oled/products/index.htm

[63] A. E. Kelly *et al.*, "High-speed GaN micro-LED arrays for data communications," in *Proc. 14th Int. Conf. Transparent Opt. Netw. (ICTON)*, Coventry, U.K., Jul. 2012, pp. 1–5.

[64] R. Zhang and H. S.-H. Chung, "A TRIAC-dimmable LED lamp driver with wide dimming range," *IEEE Trans. Power Electron.*, vol. 29, no. 3, pp. 1434–1446, Sep. 2014.

[65] I. Akasaki, H. Amano, and S. Nakamura. (2014). *Efficient Blue Light-Emitting Diodes Leading to Bright and Energy-Saving White Light Sources*. [Online]. Available: https://www.nobelprize.org/nobel-prizes/physics/laureates/2014/advanced-physicsprize2014-2.pdf

[66] T.-J. Liang, W.-J. Tseng, J.-F. Chen, and J.-P. Wu, "A novel line frequency multistage conduction LED driver with high power factor," *IEEE Trans. Power Electron.*, vol. 30, no. 9, pp. 5103–5115, Sep. 2015.

[67] R. Y. Mesleh, H. Haas, S. Sinanovic, C. W. Ahn, and S. Yun, "Spatial modulation," *IEEE Trans. Veh. Technol.*, vol. 57, no. 4, pp. 2228–2241, Jul. 2008.

[68] R. J. Drost and B. M. Sadler, "Constellation design for color-shift keying using billiards algorithms," in *Proc. IEEE GLOBECOM Workshops*, Miami, FL, USA, Dec. 2010, pp. 980–984.

[69] J. Armstrong and B. Schmidt, "Comparison of asymmetrically clipped optical OFDM and DC-biased optical OFDM in AWGN," *IEEE Commun. Lett.*, vol. 12, no. 5, pp. 343–345, May 2008.

[70] Q. Wang, C. Qian, X. Guo, Z. Wang, D. G. Cunningham, and I. H. White, "Layered ACO-OFDM for intensity-modulated direct-detection optical wireless transmission," *Opt. Exp.*, vol. 23, no. 9, pp. 12382–12393, May 2015.

[71] K. Lee and H. Park, "Modulations for visible light communications with dimming control," *IEEE Photon. Technol. Lett.*, vol. 23, no. 16, pp. 1136–1138, Aug. 15, 2011.

[72] Q. Wang, Z. Wang, and L. Dai, "Asymmetrical hybrid optical OFDM for visible light communications with dimming control," *IEEE Photon. Technol. Lett.*, vol. 27, no. 9, pp. 974–977, May 1, 2015.

[73] J. B. Carruthers and J. M. Kahn, "Multiple-subcarrier modulation for nondirected wireless infrared communication," *IEEE J. Sel. Areas Commun.*, vol. 14, no. 3, pp. 538–546, Apr. 1996.

[74] J. Armstrong, B. Schmidt, D. Kalra, H. A. Suraweera, and A. J. Lowery, "SPC07-4: Performance of asymmetrically clipped optical OFDM in AWGN for an intensity modulated direct detection system," in *Proc. IEEE Global Telecommun. Conf. (GLOBECOM)*, Nov. 2006, pp. 1–5.

[75] X. Li, R. Mardling, and J. Armstrong, "Channel capacity of IM/DD optical communication systems and of ACO-OFDM," in *Proc. IEEE ICC*, Glasgow, Scotland, Jun. 2007, pp. 2128–2133.

[76] S. Tian, K. Panta, H. A. Suraweera, B. Schmidt, S. Mclaughlin, and J. Armstrong, "A novel timing synchronization method for ACO-OFDM-based optical wireless communications," *IEEE Trans. Wireless Commun.*, vol. 7, no. 12, pp. 4958–4967, Dec. 2008.

[77] J. Armstrong, "OFDM for optical communications," *IEEE J. Lightw. Technol.*, vol. 27, no. 3, pp. 189–204, Feb. 1, 2009.

[78] S. K. Wilson and J. Armstrong, "Transmitter and receiver methods for improving asymmetrically-clipped optical OFDM," *IEEE Trans. Wireless Commun.*, vol. 8, no. 9, pp. 4561–4567, Sep. 2009.

[79] D. J. F. Barros and J. M. Kahn, "Comparison of orthogonal frequency-division multiplexing and ON–OFF keying in direct-detection multimode fiber links," *J. Lightw. Technol.*, vol. 29, no. 15, pp. 2299–2309, Aug. 1, 2011.
[80] S. D. Dissanayake and J. Armstrong, "Novel techniques for combating DC offset in diversity combined ACO-OFDM," *IEEE Commun. Lett.*, vol. 15, no. 11, pp. 1237–1239, Nov. 2011.
[81] X. Li, J. Vucic, V. Jungnickel, and J. Armstrong, "On the capacity of intensity-modulated direct-detection systems and the information rate of ACO-OFDM for indoor optical wireless applications," *IEEE Trans. Commun.*, vol. 60, no. 3, pp. 799–809, Mar. 2012.
[82] D. J. F. Barros, S. K. Wilson, and J. M. Kahn, "Comparison of orthogonal frequency-division multiplexing and pulse-amplitude modulation in indoor optical wireless links," *IEEE Trans. Commun.*, vol. 60, no. 1, pp. 153–163, Jan. 2012.
[83] R. Zhang and L. Hanzo, "Multi-layer modulation for intensity-modulated direct-detection optical OFDM," *IEEE/OSA J. Opt. Commun. Netw.*, vol. 5, no. 12, pp. 1402–1412, Dec. 2013.
[84] S. D. Dissanayake and J. Armstrong, "Comparison of ACO-OFDM, DCO-OFDM and ADO-OFDM in IM/DD systems," *J. Lightw. Technol.*, vol. 31, no. 7, pp. 1063–1072, Apr. 1, 2013.
[85] B. Ranjha and M. Kavehrad, "Hybrid asymmetrically clipped OFDM-based IM/DD optical wireless system," *IEEE/OSA J. Opt. Commun. Netw.*, vol. 6, no. 4, pp. 387–396, Apr. 2014.
[86] J. Jiang, P. Zhang, R. Zhang, S. Chen, and L. Hanzo, "Aperture selection for ACO-OFDM in free-space optical turbulence channel," *IEEE Trans. Veh. Technol.*, to be published.
[87] W. Popoola, E. Poves, and H. Haas, "Generalised space shift keying for visible light communications," in *Proc. 8th Int. Symp. Commun. Syst., Netw. Digit. Signal Process. (CSNDSP)*, Poznań, Poland, Jul. 2012, pp. 1–4.
[88] W. O. Popoola, E. Poves, and H. Haas, "Error performance of generalised space shift keying for indoor visible light communications," *IEEE Trans. Commun.*, vol. 61, no. 5, pp. 1968–1976, Mar. 2013.
[89] L. Zeng, D. O'Brien, H. Le-Minh, K. Lee, D. Jung, and Y. Oh, "Improvement of date rate by using equalization in an indoor visible light communication system," in *Proc. 4th IEEE Int. Conf. Circuits Syst. Commun.*, May 2008, pp. 678–682.
[90] T. Komine, J. H. Lee, S. Haruyama, and M. Nakagawa, "Adaptive equalization system for visible light wireless communication utilizing multiple white LED lighting equipment," *IEEE Trans. Wireless Commun.*, vol. 8, no. 6, pp. 2892–2900, Jun. 2009.
[91] K. Fan, T. Komine, Y. Tanaka, and M. Nakagawa, "The effect of reflection on indoor visible-light communication system utilizing white LEDs," in *Proc. 5th Int. Symp. Wireless Pers. Multimedia Commun.*, 2002, pp. 611–615.
[92] P. Chvojka, S. Zvanovec, P. A. Haigh, and Z. Ghassemlooy, "Channel characteristics of visible light communications within dynamic indoor environment," *IEEE J. Lightw. Technol.*, vol. 33, no. 9, pp. 1719–1725, May 1, 2015.
[93] L. Zeng *et al.*, "High data rate multiple input multiple output (MIMO) optical wireless communications using white LED lighting," *IEEE J. Sel. Areas Commun.*, vol. 27, no. 9, pp. 1654–1662, Dec. 2009.
[94] A. H. Azhar, T. Tran, and D. O'Brien, "A gigabit/s indoor wireless transmission using MIMO-OFDM visible-light communications," *IEEE Photon. Technol. Lett.*, vol. 25, no. 2, pp. 171–174, Jan. 15, 2013.
[95] T. Q. Wang, Y. A. Sekercioglu, and J. Armstrong, "Analysis of an optical wireless receiver using a hemispherical lens with application in MIMO visible light communications," *IEEE J. Lightw. Technol.*, vol. 31, no. 11, pp. 1744–1754, Apr. 12, 2013.
[96] Y. Hong, J. Chen, Z. Wang, and C. Yu, "Performance of a precoding MIMO system for decentralized multiuser indoor visible light communications," *IEEE Photon. J.*, vol. 5, no. 4, Aug. 2013, Art. ID 7800211.
[97] K.-H. Park, Y.-C. Ko, and M. Alouini, "On the power and offset allocation for rate adaptation of spatial multiplexing in optical wireless MIMO channels," *IEEE Trans. Commun.*, vol. 61, no. 4, pp. 1535–1543, Apr. 2013.
[98] T. Fath and H. Haas, "Performance comparison of MIMO techniques for optical wireless communications in indoor environments," *IEEE Trans. Commun.*, vol. 61, no. 2, pp. 733–742, Feb. 2013.
[99] Y. Wang and N. Chi, "Demonstration of high-speed 2×2 non-imaging MIMO Nyquist single carrier visible light communication with frequency domain equalization," *J. Lightw. Technol.*, vol. 32, no. 11, pp. 2087–2093, Jun. 1, 2014.
[100] T. Chen, L. Liu, B. Tu, Z. Zheng, and W. Hu, "High-spatial-diversity imaging receiver using fisheye lens for indoor MIMO VLCs," *IEEE Photon. Technol. Lett.*, vol. 26, no. 22, pp. 2260–2263, Nov. 15, 2014.
[101] M. Biagi, A. M. Vegni, S. Pergoloni, P. M. Butala, and T. D. C. Little, "Trace-orthogonal PPM-space time block coding under rate constraints for visible light communication," *J. Lightw. Technol.*, vol. 33, no. 2, pp. 481–494, Jan. 15, 2015.
[102] Q. Wang, Z. Wang, and L. Dai, "Multiuser MIMO-OFDM for visible light communications," *IEEE Photon. J.*, vol. 7, no. 6, Dec. 2015, Art. ID 7904911.
[103] A. H. Azhar, T.-A. Tran, and D. O'Brien, "Demonstration of high-speed data transmission using MIMO-OFDM visible light communications," in *Proc. IEEE GLOBECOM Workshops*, Dec. 2010, pp. 1052–1056.
[104] K. D. Dambul, D. O'Brien, and G. Faulkner, "Indoor optical wireless MIMO system with an imaging receiver," *IEEE Photon. Technol. Lett.*, vol. 23, no. 2, pp. 97–99, Jan. 15, 2010.
[105] J. Armstrong and A. J. Lowery, "Power efficient optical OFDM," *Electron. Lett.*, vol. 42, no. 6, pp. 370–372, Mar. 2006.
[106] S. Dimitrov, S. Sinavonvic, and H. Haas, "Clipping noise in OFDM-based optical wireless communication system," *IEEE Trans. Commun.*, vol. 60, no. 4, pp. 1072–1081, Apr. 2012.
[107] M. Shreedhar and G. Varghese, "Efficient fair queuing using deficit round-robin," *IEEE/ACM Trans. Netw.*, vol. 4, no. 3, pp. 375–385, Jun. 1996.
[108] *Advanced Video Coding*, document ITU-T Rec. H.264, ITU-T, Feb. 2014.
[109] *High Efficiency Video Coding for Generic Audiovisual Services*, document ITU-T Rec. H.265, ITU-T, Apr. 2015.
[110] S. Le Digabel, "Algorithm 909: NOMAD: Nonlinear optimization with the MADS algorithm," *ACM Trans. Math. Soft.*, vol. 37, no. 4, Feb. 2011, Art. ID 44.
[111] L. L. Hanzo, C. H. Wong, and M. S. Yee, *Adaptive Wireless Transceivers: Turbo-Coded, Turbo-Equalized and Space-Time Coded TDMA, CDMA, and OFDM Systems*. New York, NY, USA: Wiley, Mar. 2002, p. 752.
[112] Y. Huo, C. Hellge, T. Wiegand, and L. Hanzo, "A tutorial and review on inter-layer FEC coded layered video streaming," *IEEE Commun. Surveys Tuts.*, vol. 17, no. 2, pp. 1166–1207, 2015. AQ:10
[113] Y. Huo, M. El-Hajjar, and L. Hanzo, "Wireless video: An interlayer error-protection-aided multilayer approach," *IEEE Veh. Technol. Mag.*, vol. 9, no. 3, pp. 104–112, Sep. 2014.
[114] Y. Huo, M. El-Hajjar, R. G. Maunder, and L. Hanzo, "Layered wireless video relying on minimum-distortion inter-layer FEC coding," *IEEE Trans. Multimedia*, vol. 16, no. 3, pp. 697–710, Apr. 2014.
[115] Y. Huo, T. Wang, R. G. Maunder, and L. Hanzo, "Iterative source and channel decoding relying on correlation modelling for wireless video transmission," *IET Commun.*, vol. 7, no. 14, pp. 1465–1475, 2013.
[116] L. Hanzo, R. Maunder, T. Wang, and Y. Huo, "Motion-aware mesh-structured trellis for correlation modelling aided distributed multi-view video coding," *IEEE Trans. Image Process.*, vol. 23, no. 1, pp. 319–331, Jan. 2014.
[117] C. Zhu, Y. Huo, B. Zhang, R. Zhang, M. El-Hajjar, and L. Hanzo, "Adaptive truncated HARQ aided layered video streaming relying on inter-layer FEC coding," *IEEE Trans. Veh. Technol.*, to be published.
[118] H. Chen, R. G. Maunder, and L. Hanzo, "Low-complexity multiple-component turbo-decoding-aided hybrid ARQ," *IEEE Trans. Veh. Technol.*, vol. 60, no. 4, pp. 1571–1577, May 2011.
[119] H. Chen, R. Maunder, Y. Ma, R. Tafazolli, and L. Hanzo, "Hybrid-ARQ-aided short fountain codes designed for block-fading channels," *IEEE Trans. Veh. Technol.*, vol. 64, no. 12, pp. 5701–5712, Dec. 2015.
[120] B. Zhang, H. Chen, M. El-Hajjar, R. Maunder, and L. Hanzo, "Distributed multiple-component turbo codes for cooperative hybrid ARQ," *IEEE Signal Process. Lett.*, vol. 20, no. 6, pp. 599–602, Jun. 2013.
[121] H. Chen, R. G. Maunder, and L. Hanzo, "A survey and tutorial on low-complexity turbo coding techniques and a holistic hybrid ARQ design example," *IEEE Commun. Surveys Tuts.*, vol. 15, no. 4, pp. 1546–1566, 2013.

IEEE Access
The journal for rapid open access publishing

JUNYI JIANG received the B.Eng. degree in communication engineering from the Heilongjiang Institute of Science and Technology, in 2009, and the M.Sc. (Hons.) degree in wireless communication from the University of Southampton, U.K., in 2010, where he is currently pursuing the Ph.D. degree with the Wireless Group.

His research interests include indoor visible light communication, free-space optical communication, and iterative detection.

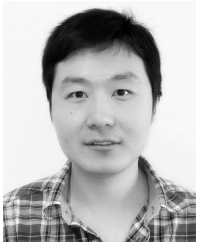

YONGKAI HUO received the B.Eng. (Hons.) degree in computer science and technology from the Hefei University of Technology, Hefei, China, in 2006, the M.Eng. degree in computer software and theory from the University of Science and Technology of China, Hefei, in 2009, and the Ph.D. degree with the Wireless Communications Group, School of Electronics and Computer Science, University of Southampton, Southampton, U.K., in 2014. He is currently a Research Fellow with the University of Southampton. His research interests include distributed video coding, multiview video coding, robust wireless video streaming, and joint source-channel decoding. He received a scholarship under the China-U.K. Scholarships for Excellence Program.

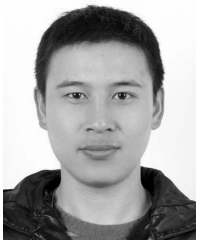

FAN JIN received the B.Sc. degree from the Huazhong University of Science and Technology, China, and the Ph.D. degree from Southampton University, U.K. He is currently an Engineer in Huawei, China. His research interests include multiuser communications, radio resource allocation, spectrum sensing, and interference management in femtocells and heterogeneous networks. He has received a scholarship under the U.K.-China Scholarships for Excellence Program.

PEICHANG ZHANG received the B.Eng. (Hons.) degree in electronics engineering from the University of Central Lancashire, Lancashire, U.K., in 2009, the M.Sc. (Hons.) degree in wireless Communications from the University of Southampton, Southampton, U.K., in 2010, and the Ph.D. degree from the Communications Signal Processing, and Control Research Group, Department of Electronics and Computer Science, University of Southampton. He holds a lecturing position with the Department of CIE, Shenzhen University, China. His research interests include coherent and non-coherent detection, and iterative detection and estimation.

ZHAOCHENG WANG (M'09–SM'11) received the B.S., M.S., and Ph.D. degrees from Tsinghua University, Beijing, China, in 1991, 1993, and 1996, respectively. From 1996 to 1997, he was a Post-Doctoral Fellow with Nanyang Technological University, Singapore. From 1997 to 1999, he was with the OKI Techno Centre (Singapore) Pte. Ltd., Singapore, where he was firstly a Research Engineer and later became a Senior Engineer. From 1999 to 2009, he was with Sony Deutschland GmbH, where he was firstly a Senior Engineer and later became a Principal Engineer. He is currently a Professor with the Department of Electronic Engineering, Tsinghua University, and serves as the Director of the Broadband Communication Key Laboratory with the Tsinghua National Laboratory for Information Science and Technology. He has authored or co-authored over 100 international journal papers (SCI indexed). He holds 34 granted U.S./EU patents. He co-authored two books, one of them with the title of *Millimeter Wave Communication Systems* (Wiley- IEEE Press), was selected by the IEEE Series on Digital & Mobile Communication. His research areas include wireless communications, millimeter-wave communications, visible light communications, and digital broadcasting. He is a fellow of The Institution of Engineering and Technology. He has served as the Associate Editor of the IEEE TRANSACTIONS ON WIRELESS COMMUNICATIONS and the IEEE COMMUNICATIONS LETTERS, and has also served as the Technical Program Committee Co-Chair of various international conferences.

ZHENGYUAN XU received the B.S. and M.S. degrees from Tsinghua University, Beijing, China, in 1989 and 1991, respectively, and the Ph.D. degree from the Stevens Institute of Technology, NJ, USA, in 1999. From 1991 to 1996, he was with the Tsinghua Unisplendour Group Corporation, Tsinghua University, as a System Engineer and Department Manager. In 1999, he joined the University of California at Riverside, first as an Assistant Professor and then a Tenured Associate Professor and Professor. He was the Founding Director of the multi-campus Center for Ubiquitous Communication by Light, University of California. In 2010, he was selected by the Thousand Talents Program of China, appointed as a Professor with Tsinghua University, and then joined the University of Science and Technology of China (USTC). He is the Founding Director of the Optical Wireless Communication and Network Center and the Wireless-Optical Communications Key Laboratory with the Chinese Academy of Sciences, and the Vice Dean of the School of Information Science and Technology with USTC. He is also a Chief Scientist of the National Key Basic Research Program (973 Program) of China. He has authored over 200 journal and conference papers. His research focuses on wireless communication and networking, optical wireless communications, geolocation, intelligent transportation, and signal processing. He has served as an Associate Editor and a Guest Editor for different IEEE and OSA journals. He was a Founding Chair of the IEEE Workshop on Optical Wireless Communications.

HARALD HAAS received the Ph.D. degree from the University of Edinburgh, in 2001. He currently holds the Chair of Mobile Communications with the University of Edinburgh, and is the Co-Founder and Chief Scientific Officer with pureLiFi Ltd., and the Director of the LiFi Research and Development Center with the University of Edinburgh. He first introduced and coined spatial modulation and LiFi. LiFi was listed among the 50 best inventions in *TIME Magazine* 2011. His main research interests are in optical wireless communications, hybrid optical wireless and RF communications, spatial modulation, and interference coordination in wireless networks.

Prof. Haas was an Invited Speaker at TED Global 2011, and his talk: Wireless Data from Every Light Bulb has been watched online more than 2 million times. He gave a second TED Global lecture on the use of solar cells as LiFi data detectors and energy harvesters in 2015. This has been viewed online more than 650 000 times within one month. He holds 31 patents and over 30 pending patent applications. He has authored 300 conference and journal papers, including a paper in Science. He co-authored a book entitled *Principles of LED Light Communications Toward Networked Li-Fi* (Cambridge University Press, 2015). He was a co-recipient of recent best paper awards at the IEEE Vehicular Technology Conference (VTC) in Las Vegas in 2013 Fall, and VTC in Glasgow in 2015 Spring. He was also a co-recipient of the EURASIP Best Paper Award for the *Journal on Wireless Communications and Networking* in 2015, and the Jack Neubauer Memorial Award of the IEEE Vehicular Technology Society. In 2012, he was a recipient of the prestigious Established Career Fellowship from the Engineering and Physical Sciences Research Council (EPSRC) within Information and Communications Technology in the U.K. He is a recipient of the Tam Dalyell Prize 2013 by the University of Edinburgh for excellence in engaging the public with science. In 2014, he was selected by EPSRC as one of ten Recognizing Inspirational Scientists and Engineers Leaders in the U.K.

LAJOS HANZO (F'–) received the degree in electronics in 1976, the Ph.D. degree in 1983, the Doctor Honoris Causa degree from the Technical University of Budapest, in 2009, and the D.Sc. degree. During his 38-year career in telecommunications, he has held various research and academic positions in Hungary, Germany, and U.K. Since 1986, he has been with the School of Electronics and Computer Science, University of Southampton, U.K., as the Chair in Telecommunications. He has 22 000+ citations. He has successfully supervised 100 Ph.D. students, co-authored 20 *Mobile Radio Communications* (John Wiley/IEEE Press) books totaling in excess of 10 000 pages, authored over 1500 research entries at the IEEE Xplore, acted as the TPC Chair and General Chair of the IEEE conferences, presented keynote lectures, and received a number of distinctions. He is directing 60 strong academic research teams, working on a range of research projects in the field of wireless multimedia communications sponsored by the industry, the Engineering and Physical Sciences Research Council, U.K., the European Research Council's Advanced Fellow Grant, and the Royal Society's Wolfson Research Merit Award. He is an enthusiastic supporter of industrial and academic liaison. He offers a range of industrial courses. He is also a Governor of the IEEE VTS. From 2008 to 2012, he was the Editor-in-Chief of the *IEEE Press* and a Chaired Professor with Tsinghua University, Beijing. His research is funded by the European Research Council's Senior Research Fellow Grant. He is a fellow of REng, IET, and EURASIP.

AUTHOR QUERIES

AQ:1 = Please check whether the edits made in the financial section are OK.
AQ:2 = The words ‘‘optimisation,’’ ‘‘minimising,’’ and ‘‘characterising’’ has been changed to ‘‘optimization,’’ ‘‘minimizing,’’ and ‘‘characterizing’’ as per U.S. style, respectively. Please ensure that it is carried out in the rest of the article.
AQ:3 = Please confirm whether the section headings are appropriate as set.
AQ:4 = Please provide the issue no. for ref. [1].
AQ:5 = Please confirm the volume no. for refs. [7], [16], [36], and [40].
AQ:6 = Please provide the volume no., issue no., page range, month, and year for refs. [8], [86], and [117].
AQ:7 = Please provide the author name and paper no. for ref. [10].
AQ:8 = Please provide the organization location for ref. [32].
AQ:9 = Please provide the accessed date for ref. [33].
AQ:10 = Please provide the month for refs. [112] and [121].
AQ:11 = Current affiliation in biography of ‘‘PEICHANG ZHANG, ZHAOCHENG WANG, ZHENGYUAN XU, and HARALD HAAS’’ do not match First Footnote. Please check.
AQ:12 = Please provide the membership year for the author ‘‘Lajos Hanzo.’’